Biogeochemistry (2023) 163:219–243
https://doi.org/10.1007/s10533-023-01021-2

RESEARCH

Transitions in nitrogen and organic matter form and concentration correspond to bacterial population dynamics in a hypoxic urban estuary

Georgie E. Humphries · Jessica I. Espinosa · Mariapaola Ambrosone · Zabdiel Roldan Ayala · Maria Tzortziou · Joaquim I. Goes · Dianne I. Greenfield

Received: 26 September 2022 / Accepted: 18 January 2023 / Published online: 25 February 2023

Abstract Nitrogen (N) inputs to developed coastlines are linked with multiple ecosystem and socioeconomic impacts worldwide such as algal blooms, habitat/resource deterioration, and hypoxia. This study investigated the microbial and biogeochemical processes associated with recurrent, seasonal bottom-water hypoxia in an urban estuary, western Long Island Sound (WLIS), that receives high N inputs. A 2-year (2020–2021) field study spanned two hypoxia events and entailed surface and bottom depth water sampling for dissolved nutrients as inorganic N (DIN; ammonia-N and nitrite + nitrate (N + N)), organic N, orthophosphate, organic carbon (DOC), as well as chlorophyll *a* and bacterial abundances. Physical water quality data were obtained from concurrent conductivity, temperature, and depth casts. Results showed that dissolved organic matter was highest at the most-hypoxic locations, DOC was negatively and significantly correlated with bottom-water dissolved oxygen (Pearson's $r = -0.53$, $p = 0.05$), and ammonia-N was the dominant DIN form pre-hypoxia before declining throughout hypoxia. N + N concentrations showed the reverse, being minimal pre-hypoxia then increasing during and following hypoxia, indicating that ammonia oxidation likely contributed to the switch in dominant DIN forms and is a key pathway in WLIS water column nitrification. Similarly, at the most hypoxic sampling site, bottom depth bacteria concentrations ranged ~ 1.8×10^4–1.1×10^5 cells ml^{-1} pre-hypoxia, declined throughout hypoxia, and were positively and significantly correlated (Pearson's $r = 0.57$; $p = 0.03$) with ammonia-N, confirming that hypoxia influences N-cycling within LIS. These

Responsible Editor: Scott Neubauer

Supplementary Information The online version contains supplementary material available at https://doi.org/10.1007/s10533-023-01021-2.

G. E. Humphries · Z. R. Ayala · D. I. Greenfield (✉)
School of Earth and Environmental Sciences, Queens College, Queens, NY 11367, USA
e-mail: dgreenfield@gc.cuny.edu

G. E. Humphries · J. I. Espinosa · M. Ambrosone · Z. R. Ayala · D. I. Greenfield
Advanced Science Research Center at the Graduate Center, New York, NY 10031, USA

J. I. Espinosa
Department of Ecology and Evolutionary Biology, University of Connecticut, Storrs, CT 06269, USA

M. Tzortziou
City College Center for Discovery and Innovation, New York, NY 10031, USA

M. Tzortziou
Department of Earth and Atmospheric Sciences, City College of New York, New York, USA

J. I. Goes
Lamont-Doherty Earth Observatory, Palisades, NY 10964, USA

findings provide novel insight to feedbacks between major biogeochemical (N and C) cycles and hypoxia in urban estuaries.

Keywords Bacteria · Nitrification · Hypoxia · Dissolved organic carbon · Long Island Sound

Introduction

The Long Island Sound (LIS) estuary, located between the southern coast of Connecticut (CT) and Long Island, New York (NY), is approximately 160 × 30 km (length x width), has an average depth of 20–21 m, and a principal tidal exchange with the Atlantic Ocean in its eastern portion (Gay et al. 2004). LIS is a river-dominated estuary with three major hydrographic regions: eastern (ELIS), central (CLIS), and western (WLIS), that receive freshwater from the Connecticut, Quinnipiac, and both Hudson and East Rivers, respectively, in addition to precipitation and groundwater (Gay et al. 2004; Vlahos and Whitney 2017). LIS was designated an estuary of national significance by the United States Congress in 1987 due to its large biodiversity and multiple ecosystem services (New York State Department of Environmental Conservation (NYSDEC) 2000; Latimer et al. 2014). The region is home to approximately 9.8 and 2.3 million residents in the NY and CT counties, respectively, bordering the estuary (U.S. Census 2020).

Due to urbanization surrounding the LIS watershed and its proximity to New York City (NYC), WLIS receives elevated nutrient loading (especially nitrogen (N)) from industrial and wastewater (sewer) sources (Gay et al. 2004; Long Island Sound Study 2015; Burke Watson et al. 2018; Connecticut Department of Energy and Environmental Protection (CTDEEP) 2019). When combined with atmospheric deposition, fertilizer runoff (Vaudrey et al. 2016), and other terrestrial sources, elevated N has been directly linked to recurrent (since the 1970s) eutrophication, bottom-water hypoxia (categorized by CTDEEP as dissolved oxygen (DO) < 3.00 mg l^{-1}), and occasionally anoxia (DO < 1.00 mg l^{-1}) (Koppelman et al. 1976; Welsch and Eller 1991; Ballestero et al. 2018; CTDEEP 2019). WLIS hypoxia typically occurs during the summer from Jul to Aug (Parker and O'Reilly 1991; NYSDEC 2000; Vaudrey 2017; Ballestero et al. 2018) and presents a chronic ecological risk that threatens LIS biodiversity and ecosystem resources (Cuomo et al. 2005; Pearce and Balcom 2005; CTDEEP 2019). For example, prolonged (2-Jul through 21-Aug 1999) hypoxia covered 120 mi^2 (311 km^2) and led to a stress-induced mass mortality event of WLIS lobster populations (Cuomo et al. 2005; Pearce and Balcom 2005). Thus, N-loading and subsequent hypoxia threaten LIS ecosystems and fisheries.

In 2001, the Environmental Protection Agency (EPA) implemented a total maximum daily load (TMDL) for total N (TN), with a goal of reducing NY and CT point-source TN inputs by 58.5% by August 2014 (NYSDEC 2000; Long Island Sound Study 2015). In response, refinements and upgrades to wastewater treatment facilities decreased TN-loading by 0.06 mg l^{-1} per decade, and LIS summer bottom DO has been increasing by ~ 0.48 mg l^{-1} per decade (Whitney and Vlahos 2021), decreasing the average hypoxia area by > 50%. Despite these improvements, WLIS water quality received a failing grade (43%) in 2022 (Save the Sound 2022) due to interannual variability in open water indicators as excessive productivity and seasonal hypoxia persist (O'Shea and Brosnan 2000; Burke Watson et al. 2018; Tetra Tech 2020). Point-source TN inputs remain highest in the WLIS, with a combined total equalized average daily load of 1.83×10^4 pounds (8.30×10^3 kg) in 2021 (Long Island Sound Study 2021). These inputs are major factors that make WLIS the largest TN sink of all three LIS regions, with 97% sequestered by sediment burying or degassed through denitrification, contributing to an average inferred internal N loss rate of 5.40 g N m^2 y^{-1} across the estuary (Vlahos and Whitney 2017; Vlahos et al. 2020). By comparison, CLIS and ELIS consume approximately 90% and 28% of TN, respectively, due to increasing tidal exchange with, and thus N-export to, the Atlantic Ocean and adjacent shelf, delivering 10.80×10^6 kg N y^{-1} (Vlahos et al. 2020).

Of the TN pool, dissolved inorganic nitrogen (DIN) concentrations are typically higher in WLIS than ELIS and CLIS due to heightened secondary wastewater treatment plant discharge from the NYC area (Parker and O'Reilly 1991; Gobler et al. 2006). Allochthonous DIN inputs (specifically ammonium, NH_4^+) following heavy precipitation have been coupled with WLIS hypoxia timing and severity (Anderson and Taylor 2001). In bottom waters, nitrifiers oxidize ammonium (NH_4^+) or ammonia

(NH_3) into nitrite (NO_2^-) then nitrate (NO_3^-), a process that has been associated with increased oxygen demand in estuaries (Dai et al. 2006; Garnier et al. 2007). Ammonia-N (NH_4^+ and NH_3) availability is further elevated by microbial decomposition of N-rich organic matter (OM) in sediments (Lapota et al. 2000; Borsuk et al. 2001; Staroscik and Smith 2004), amplifying sediment oxygen demand (SOD) and therefore hypoxia (Borsuk et al. 2001). In low DO (but not anoxic) environments, heightened NH_4^+ concentrations may help catalyze ammonia oxidation ($NH_3 \rightarrow NO_2^-$), the first rate limiting step of nitrification, thereby increasing NO_2^- concentrations (Lehtovirta-Morley 2018). Recent temporal patterns in DIN forms, concentrations, and their associations with bacterial abundances are largely unreported for WLIS.

Dissolved organic matter (DOM) concentrations, consisting of dissolved organic N, carbon, and phosphorus (DON, DOC, and DOP, respectively), can scale positively with microbial degradation rates (Lønborg et al. 2009). Heterotrophic bacteria metabolize DOM for growth and respiration (Moran et al. 1999; Staroscik and Smith 2004; Kamjunke et al. 2019), especially by the uptake of reduced C from DOC (Raymond and Bauer 2000; Buchan et al. 2014; Logue et al. 2016). Enhanced microbial respiration due to OM breakdown, has been associated with low DO (Parker and O'Reilly 1991; D'Sa and DiMarco 2009; Su et al. 2020), and it significantly contributes to hypoxia formation and maintenance (Parker and O'Reilly 1991; Diaz and Rosenberg 2008; Su et al. 2017). In LIS, DOM concentrations, as well as DIN (NYSDEC 2000), precipitation, low summer DO solubility, and water column stratification (determining sensitivity to hypoxia in coastal waters generally; Jensen et al. 1990; Howarth et al. 2011) have accentuated hypoxia by increasing biological oxygen demand (BOD) (Anderson and Taylor 2001; Lee and Lwiza 2008; Liu et al. 2015). Over 75% of DOM total fluorescence in WLIS is attributed to terrestrial sources, indicating that the overall DOM pool is primarily of terrigenous rather than marine origin (Schartup et al. 2015; Supino 2020), though UV–Vis evaluations of Connecticut River DOM contributions to LIS may be over-estimates due to the influence of ferric iron (Logozzo et al. 2022).

Estuarine DOC bioavailability depends on its source and environmental factors since anthropogenic and terrestrial inputs to urban systems (e.g., wastewater discharge and marsh export) can increase DOM bioavailability, especially after exposure to sunlight (Tzortziou et al. 2007; Schartup et al. 2015; Supino 2020; Logozzo et al. 2021, 2022). Urbanized LIS regions produce greater quantities of labile DOM, leading to net increases in microbial degradation rates (Supino 2020). LIS total organic C concentrations increase with point-source wastewater discharge volume (Mullaney 2015), terrestrially-loaded freshwater flow (Walsh 1995), overall anthropogenic N-inputs (NYSDEC 2000), and precipitation (in surface waters; Willey et al. 2000) leading to ~25% of LIS oxygen consumption from the oxidation of organic C (NYSDEC 2000). Rivers and marshes supply substantial, though temporally variable, DOC to LIS, with a net DOC import generally during low flow years, a net export to the continental shelf during average/high flow years (Vlahos and Whitney 2017; Byrd et al. 2020; Supino 2020), and most DOC removed via photo-oxidation (Zhong and Wang 2009). As such, terrestrial sources of labile and overall organic C levels have increased within WLIS (Varekamp 2010) coincident with a general rise in DOC concentrations throughout Northern U.S. surface waters (Evans et al. 2005).

In contrast to literature describing LIS hypoxia spatial and temporal extent, the associated microbial communities remain surprisingly understudied. Bacterial assemblages have exhibited annual cycles with summer maxima. As examples, bacterial abundances at the most-frequently hypoxic WLIS station (A4; Fig. 1) ranged $5.9–287 \times 10^8$ cells l^{-1} year-round (1996–1998) (Taylor et al. 2003), and bacterial biomass at surface depths increased (Jul–Aug of 1992–1993) coincident with rising temperatures, followed by bottom depth peaks in late Jul/early Aug (Anderson and Taylor 2001). Similarly, outputs from a coupled physical-biogeochemical model showed that WLIS simulated bacterial biomass density (per unit volume) begins to increase during Apr, fluctuates late spring-early summer, reaching 2.75 mmol N m^{-3} in Jul and 2 mmol N m^{-3} in Aug before decreasing during the fall (Liu et al. 2015). While less is known about WLIS microbial diversity, high-throughput sequencing using 16S rRNA genes revealed that spatial and temporal trends in dominant taxa coincided with bottom-water hypoxia during 2019 (Santoferrara et al. 2022).

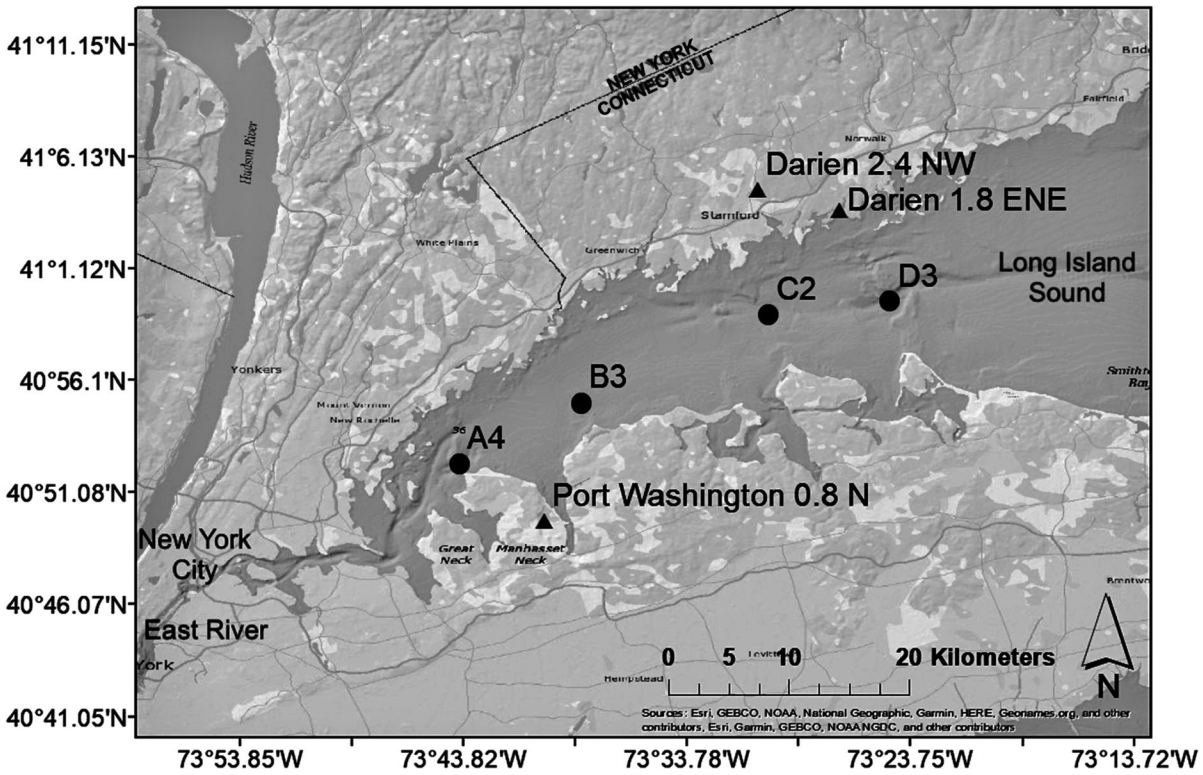

Fig. 1 Map of WLIS sampling stations (circle markers) A4 (40.972500, − 73.734167, Execution Rocks NY), B3 (40.918333, − 73.642833, Rye Beach NY), C2 (40.984333, − 73.502167, Stamford CT), and D3 (40.993833, − 73.411333, Eatons Neck Point CT). NOAA weather stations (triangles) include Port Washington 0.8 N (forecast area: 40.838800, − 73.669722), Darien 2.4 NW (forecast area: 41.077222, − 73.510200), and 1.8 ENE (forecast area: 41.062222, − 73.448889)

Connections between WLIS bacterial populations and phytoplankton biomass (chlorophyll (chl) *a*) are poorly understood. These are important considerations because phytoplankton supply autochthonous DOM to bacteria that, depending on the timing, DOM quality and quantity, could influence hypoxia onset and severity. Increases in chl *a* following DON enrichment can result in elevated DOC (Reed et al. 2015); both DOC and DON have been spatially and temporally correlated with chl *a* biomass in Long Island embayments (Lonsdale et al. 2006), and DOC quality in LIS is enriched by in situ primary production (Whitney and Vlahos 2021). Although WLIS generally exhibits higher levels of chl *a* than either CLIS or ELIS (CTDEEP 2019), variance in bacterial biomass has not been closely associated with chl *a* (Anderson and Taylor 2001; Taylor et al. 2003). Since the implementation of TMDLs, these critical microbial associations and biogeochemical processes have been largely understudied, representing a significant gap in our modern understanding of LIS hypoxia dynamics. Given the wealth of evidence that N enrichment increases phytoplankton biomass (Heisler et al. 2008; Reed et al. 2015; Glibert et al. 2018; Sitta et al. 2018; CTDEEP 2019), it is relevant to consider synergies between chl *a* and WLIS bacterial abundances.

The goal of this study was to evaluate linkages between bacterial populations, dissolved inorganic and organic N and P, DOM, and chl *a* temporal transitions during WLIS hypoxia. The primary objectives were to quantify bacterial abundances over two growing seasons (spring-winter) that encompass pre-, during, and post-hypoxia, as well as track seasonal nutrient

concentrations, chl *a*, and water quality (physical water quality, DO, precipitation). Results not only refine our understanding of biogeochemical processes and microbial dynamics associated with WLIS hypoxia timing and spatial coverage, but they are also applicable to other hypoxia-prone coastal ecosystems worldwide.

Methods and materials

Sample collection

Water sampling leveraged long-term LIS water quality (monthly, year-round) and hypoxia (bimonthly, Jun-Sep) monitoring surveys conducted by the Connecticut Department of Energy and Environmental Protection (CTDEEP). Stations, west to east across Western Long Island Sound (WLIS), spanned a gradient of decreasing bottom depth hypoxia severity and increasing distance from NYC as (depth, location) A4 (34.70 m, Execution Rocks), B3 (19.50 m, Rye Beach), C2 (33.40 m, Stamford CT), and D3 (44.60 m, Eatons Neck Point) (Fig. 1). The western-most station (A4) has experienced the highest frequency of hypoxia events, with ~ 26% of discrete DO measurements (1991–2015) from all depths < 3.00 mg l^{-1} (Ballestero et al. 2018). Additionally, anoxia (< 1.00 mg l^{-1}) has been detected as recently as Aug 2019 (0.88–0.89 mg l^{-1}; CTDEEP 2019) at A4. Of years when hypoxia was detected (1994–2020), DO at station A4 was < 3.00 mg l^{-1} 90–100% of the time (CTDEEP 2019). By comparison, during this same timeframe stations C2 and D3, which are closer to the less urbanized CLIS, experienced DO < 3.00 mg l^{-1} 60–70% and 40–50% of hypoxic years, respectively (CTDEEP 2019). During 2020, monthly (1 survey per month) water samples were collected Jul–Nov, with two surveys conducted in Jul and Aug each. COVID-19 prevented Mar–Jun 2020 surveys. During 2021, samples spanned Mar–Oct, with two surveys conducted during Jul, three during Aug, and monthly otherwise.

At each station, water samples ($n = 3$) were collected in 1 L Nalgene© amber wide-mouth bottles from surface (2 m) and bottom (−5 m from the benthos) depths. All sample collection bottles were previously soaked in 10% hydrochloric acid (HCl) for a minimum of 24 h then rinsed 3 times with reverse osmosis (RO) filtered water and 3 times with double distilled water (ddH_2O). All water samples were stored in coolers then transported to the Advanced Science Research Center, NY, for processing within 2 h of shore arrival.

Physical water quality and precipitation

At each station, in situ depth profiles were recorded using a YSI EXO2 Multiparameter Water Quality Sonde for temperature (°C), salinity (psu), pH, turbidity (FNU), and DO (mg l^{-1}). Seven-day cumulative precipitation (mm) prior to each sampling date was calculated using the National Oceanic and Atmospheric Administration's (NOAA) Climate Data Online Tool (https://www.weather.gov/wrh/Climate?wfo=okx). To locate weather stations, full map-view was employed. Weather stations were chosen based on proximity to survey stations as Port Washington 0.8 N (forecast area: 40.8388, −73.6700) corresponded to A4 and B3, and Darien 2.4 NW (forecast area: 41.0772, −73.5102) and 1.8 ENE (forecast area: 41.0619, −73.4488) corresponded to C2 and D3, respectively. The NOAA Climate Data Online Tool's "Daily data for a month" was used to gain daily precipitation measurements per sampling timeframe.

Water chemistry

Upon return to the laboratory, all samples were gently rotated ~ 10 × to ensure water was well-mixed prior to processing. Then, using a 30 ml syringe, water from each replicate was filtered through a 25 mm, 0.7 µm pore size glass fiber filter (GF/F) (Whatman®) into acid-washed (as described previously) 20 ml glass scintillation vials (~ 17 ml final volume) for DIN: nitrate + nitrite ($NO_3^- + NO_2^-$; henceforth N + N, ammonia-N ($NH_3 + NH_4^+$; henceforth AmN), dissolved inorganic phosphorus (DIP): orthophosphate (PO_4^{3-}), total dissolved N (TDN), and phosphorus (TDP). Sample vials were then frozen (−20 °C) until analysis. Nutrient samples were analyzed within 1 h of thawing using a Hach© Lachat QuikChem 8500 Flow Injection Analysis System (Strickland and Parsons 1984; Grasshoff et al. 1999). Protocol Minimum Detection Limit (MDLs) were as follows: AmN (0.05 µM; Lachat Applications Group 2017), N + N (0.014 µM; Egan 2008), PO_4^{3-} (0.0646 µM; Egan

2007), TDN and TDP (0.485 and 0.123 µM, respectively; Tucker et al. 2008a, 2008b). MDLs were used when measured concentrations were below those values. DON and DOP concentrations were calculated per replicate as TDN–DIN and TDP–DIP, respectively. DOC samples were collected following standard procedures (Ducklow and Dickson 1994; JGOFS 1996), specifically by filtering water through a 30 ml syringe (previously soaked in 10% HCL for 24 h then rinsed 3 times with ddH_2O, equipped with a pre-combusted (2 h at 450 °C) GF/F) into a pre-combusted (4 h at 450 °C) 20 ml glass scintillation vial. Following addition of two to three drops of 10% HCl, vials containing samples were stored (4 °C) prior to analysis (in duplicates), and subsequently analyzed by the University of Wisconsin–Milwaukee. DOM was calculated as the sum of DON, DOP, and DOC.

Bacterial abundances

To quantify bacterial concentrations, water from each replicate was initially passed through a 20 µm Nitex mesh to exclude larger particles. Filtrate (27 ml) was dispensed into 50 ml amber glass vials containing 3 ml of 20% Phosphate-buffered saline (PBS) buffered formaldehyde that was added no more than 1 h beforehand (final concentration of 1.13% PBS), then the fixed samples were stored at 4 °C. To prepare 20% PBS-buffered formaldehyde stock solution (1 l), 540.5 ml of 37% formaldehyde was added to 459.5 ml of PBS buffer. PBS buffer was pre-made by dissolving one Thermo Scientific™ BupH PBS pouch of dry-blend powder with 500 ml ddH_2O to produce a 0.1 M sodium phosphate and 0.15 M sodium chloride buffer solution that was subsequently passed through a sterile 0.2 µm pore-size polyether-sulfone (PES) filter and stored in an acid-washed (as above) 500 ml glass flask at 20 °C. Thermo Fisher Scientific™ 4′,6-diamidino-2-phenylindole (DAPI) stock solution was prepared by diluting 1 mg of DAPI/1 ml ddH_2O. DAPI working solution was prepared as 100 µl DAPI stock/1 ml ddH_2O for a 10,000 µg/1 ml ddH_2O final concentration (Porter and Feig 1980). Ten 1–2 ml aliquots of DAPI working solution were stored (−20 °C) in 2 ml capped amber Eppendorf tubes. Bacterial samples were stained using 30 ml glass towers pre-rinsed with 40% ethanol followed by washing 3 times with ddH_2O then affixed with 25 mm GF/A grade backing filters for ddH_2O-washed Isopore™ 0.2 µm black polycarbonate membrane filters. Glass towers were clamped to the manifold, 2 ml of fixed sample were added to each tower followed by 20 µg DAPI working solution (10 µg/1 ml final sample), and then towers were incubated for 5 min in a darkened room and under aluminum foil caps to block light. Afterward, each tower was rinsed three additional times with 3 ml of PBS buffered formalin for a total of 4 filtrations. The stained Isopore™ black polycarbonate membrane filters were then mounted on glass slides with Corning© 25 mm glass coverslips and stored at −20 °C in the dark.

Bacterial quantification occurred within 1 week of DAPI staining using a Nikon ECLIPSE Ni upright epifluorescent microscope (DAPI excitation peak at 259 nm and emission peak at 457 nm; absorption maximum at a wavelength of 358 nm (UV)) set to manual specifications (Nikon 2015). Each mounted Isopore™ black polycarbonate membrane filter was viewed under a 40×/0.80W (400×magnification) objective lens using NIS-Elements AR 5.21.03 software. For each filtered sample, the 40×DAPI and Sola light was used to display a randomly selected 460×460 µm (211,600 μm^2) view field within the DAPI-stained region, and that square was imaged to avoid over-exposure. This procedure was repeated 14 times for a total of 15 images per filter. The NIS-Elements software automatic "Object Count" function was then used to quantify all particles within the typical marine bacterial cell diameter range (0.20–2.00 µm), and bacterial cell concentrations were quantified according to Eq. 1.

$$BacC = N \times (CF/V) \quad (1)$$

where BacC = bacterial cell concentration (cells ml^{-1}); N = total number of bacteria cells counted per 2 ml; CF = conversion factor (B_a/B_c) such that B_a = total area of filter exposed to the sample (μm^2); B_c = area of the filter quantified (μm^2); and V = volume of sample added to tower (ml). Since the diameter of the Isopore™ filter exposed to the sample was 2.00 cm (radius (r) of 1.00 cm), $B_a = \pi r^2$, or 3.10×10^8 μm^2, B_c = 15 images×211,600 μm^2 per image, or 3.20×10^6 μm^2, thus CF = 98.979. For each replicate, the total number of bacterial cells (N) per 2 ml sample volume were counted per 15 images. To correct for sample dilution, the final volume of sample (V) was 1.80 ml (2 ml–10% addition of PBS buffered

formalin (0.20 ml)). The final concentration of bacterial cells per 1.80 ml was adjusted to the concentration of bacterial cells per 1 ml (Intergovernmental Oceanographic Commission 2010), such that Eq. 1 became:

$$\mathrm{BacC} = \mathrm{N} \times (98.979/1.80) \text{ or } \mathrm{BacC} = \mathrm{N} \times (54.99)$$

Chl a

To sample for phytoplankton biomass (chl *a*), 40 ml of whole (unfiltered) water from each surface replicate was condensed on to GF/Fs using a vacuum pump at 5 mmHg. Filters containing samples were placed in 20 ml plastic scintillation vials and stored frozen (−20 °C) until extraction with 7 ml of 90% high-performance liquid chromatography (HPLC) grade acetone added to each scintillation vial then freezing (−20 °C) for 36–48 h. Extracted samples were briefly thawed to room temperature (23 °C) in the dark, and pigment concentrations (µg chl a l^{-1}) were measured using presonicated 5 ml borosilicate glass test tubes and a Turner Designs© Trilogy Laboratory Fluorometer, non-acidification module (Welschmeyer 1994; Turner Designs 2017).

Statistical analyses

RStudio software (RStudio 2022.02.3+492 "Prairie Trillium" Release for MacOS) was used for all statistical analyses. All datasets were tested for normality (Shapiro–Wilk) then $\log_{10}$ transformed prior to further analyses. Datasets were further grouped by seasons (defined by Solstices and Equinoxes), as well as by stations, both individually and pooled as typically most hypoxic stations (A4 and B3) distinct from the less hypoxic stations (C2 and D3; CTDEEP 2019). These pooled regions are also hydrographically separated by a sill between stations B3 and C2. Pearson Correlations were then used to test significant positive and negative relationships between bacterial abundances, AmN, N+N, PO_4^3, chl *a* (surface only), DO, cumulative precipitation, DOC, DON, DOP, temperature, pH, salinity, and turbidity measurements at surface and bottom depths. All *p*-values and correlation coefficients (*r*) are reported in matrix form. Two sample *t*-Tests assuming equal variances were used to assess differences in mean DO (to differentiate statistical differences in hypoxia dynamics), chl *a*, bacterial abundances, and nutrients between stations and dates. All analyses entailed a standard confidence level of 95% ($\alpha = 0.05$).

Results

Water quality

Throughout this study, water temperature (T), salinity (S), and pH followed strong seasonal cycles and west–east gradients, with lowest S and pH, and highest T in the west across both sampling years. T ranged 2.54–23.77 °C and 2.21–23.16 °C in surface and bottom depths, respectively (Table 1). Mean T for surface waters between stations were comparable within any given season (< 2.00 °C difference; Table S1). Bottom-water T was warmest at A4 during both summers then decreased eastward, but T remained similar across stations during the rest of the year (Tables 1, S2). During 2020, the thermocline was apparent at all stations 7-Jul–12-Aug before dissipating by 1-Sep. A relatively more prominent thermocline in 2021 developed 8-Jun and remained through 31-Aug (Figs. 2, 3), coincident with a halocline and persistent hypoxia at A4 and B3. Apart from A4 in 2020, a halocline developed from 7-Jul–1-Sep 2020 to 8-Jul–31-Aug 2021 at all stations. Turbidity (FNU) was consistently higher at bottom than surface depths across all stations and seasons (Table 1) and was positively and significantly correlated with T in both surface and bottom depths (Pearson's, $r = 0.62$, $p = 0.01$; $r = 0.64$ $p = 0.00$; Tables S3a, b), respectively, throughout WLIS. Bottom depth pH was positively and significantly correlated with turbidity ($r = 0.79$, $p = 0.00$), as well as negatively and significantly with T ($r = -0.63$, $p = 0.05$; Table S3b).

Concentrations of DO generally increased eastward during both years and depths such that hypoxia severity (longest duration and lowest DO measurements) was greatest at stations A4 and B3. Concentrations of DO were lowest during summers, highest during winters and springs (Tables 1, S1, S2), and ranged 6.63–12.84 mg l^{-1} at surface depths compared to 1.05–11.86 mg l^{-1} at bottom depths (Table 1). Throughout the study, DO was significantly and negatively correlated with both T (Pearson's, $r = -0.82$, $p = 0.00$; $r = -0.75$, $p = 0.00$) and turbidity ($r = -0.63$, $p = 0.01$; $r = -0.79$, $p = 0.00$) at surface and bottom depths, respectively, as well as significantly and

Table 1 Seasonal means (n=sampling dates per season) and ranges (parentheses) for surface (2 m) (top row per entry) and bottom depths (-5 m from the benthos) (bottom row per entry) for water temperature (T; °C), salinity (S; psu), pH, turbidity (Turbid; FNU), and dissolved oxygen (DO; mg l^{-1}) measurements from CTD profiles for stations A4, B3, C2, and D3. Seasons were defined by Solstices and Equinoxes for summer (Sum), fall, winter (Win), and spring (Spr) during 2020 and 2021, denoted 20 and 21, respectively. Since Win21 and Fall21 included only one sampling date, ranges were unavailable

Season	Station	T (°C)	S (psu)	pH	Turbid (FNU)	DO (mg l^{-1})
Sum20	A4	23.04 (21.26–24.54)	26.63 (26.23–26.59)	7.97 (7.67–8.15)	1.40 (1.19–1.64)	7.05 (6.29–8.27)
		20.36 (17.55–23.16)	27.34 (27.07–27.68)	7.51 (7.28–7.82)	3.39 (2.67–4.81)	2.71 (1.77–3.77)
(n=4)	B3	23.77 (22.04–24.94)	26.68 (26.51–27.07)	8.20 (8.05–8.30)	1.36 (1.07–1.79)	9.10 (8.29–9.79)
		19.90 (17.47–23.11)	27.61 (27.15–27.98)	7.62 (7.31–7.94)	3.40 (1.85–4.60)	3.59 (2.88–4.45)
	C2	23.20 (22.11–24.29)	26.76 (25.98–27.60)	8.05 (7.96–8.18)	1.15 (0.85–1.42)	7.61 (6.45–9.10)
		19.30 (16.61–22.98)	27.96 (27.49–28.39)	7.64 (7.47–7.90)	4.88 (3.48–6.53)	4.14 (3.13–5.31)
	D3	22.95 (19.13–24.82)	27.36 (27.18–27.64)	8.05 (7.83–8.20)	1.30 (0.97–1.64)	7.56 (6.68–8.55)
		19.41 (15.93–23.02)	28.19 (27.95–28.44)	7.68 (7.45–7.92)	5.05 (3.89–8.00)	4.05 (3.01–5.08)
Fall20	A4	15.77 (13.62–17.92)	26.90 (26.52–27.27)	8.28 (7.79–8.77)	0.96 (0.79–1.12)	7.84 (7.48–8.20)
		15.98 (14.03–17.93)	27.62 (27.51–27.72)	8.09 (7.81–8.37)	1.70 (1.65–1.74)	7.48 (7.32–7.63)
(n=2)	B3	15.73 (13.35–18.10)	27.59 (27.18–28.00)	8.17 (7.87–8.47)	1.03 (0.75–1.31)	8.10 (7.57–8.62)
		16.21 (14.13–18.28)	28.10 (27.86–28.33)	8.10 (7.86–8.34)	1.50 (1.16–1.83)	7.68 (7.35–8.00)
	C2	16.56 (14.50–18.61)	28.30 (28.10–28.50)	8.05 (7.86–8.24)	1.17 (0.89–1.45)	7.82 (7.29–8.35)
		16.74 (14.88–18.60)	28.51(28.50–28.52)	8.01 (7.85–8.17)	1.58 (1.51–1.65)	7.49 (7.24–7.73)
	D3	16.54 (14.45–18.63)	28.39 (28.29–28.48)	7.91 (7.90–7.92)	1.34 (1.29–1.39)	7.99 (7.52–8.46)
		16.78 (14.96–18.69)	28.54 (28.49–28.59)	7.89 (7.85–7.92)	2.29 (1.97–2.29)	7.70 (7.19–8.20)
Win21	A4	3.04	26.60	8.24	1.03	12.84
		2.48	27.23	8.14	1.07	11.80
(n=1)	B3	2.98	26.80	8.22	0.88	12.67
		2.39	27.43	8.12	1.17	11.86
	C2	2.54	27.5	8.12	0.80	11.95
		2.21	27.68	8.07	1.72	11.52
	D3	3.02	27.50	8.15	0.84	11.87
		2.27	27.71	8.09	1.83	11.47
Spr21	A4	11.82 (8.02–16.55)	26.11 (25.86–26.44)	8.91 (8.04–10.10)	1.00 (0.99–1.06)	10.06 (8.61–12.45)
		10.03 (6.52–13.63)	26.81 (26.73–26.86)	8.52 (8.04–9.32)	1.88 (1.18–3.14)	8.61 (6.48–10.33)
(n=3)	B3	11.94 (7.77–17.73)	26.40 (26.00–26.90)	8.90 (8.09–9.44)	0.95 (0.86–1.02)	11.12 (9.47–12.84)
		9.64 (5.96–13.59)	27.03 (26.88–27.15)	8.71 (8.05–9.24)	1.83 (1.13–2.76)	8.97 (7.31–10.55)
	C2	11.37 (6.11–17.66)	26.90 (26.40–27.20)	9.17 (8.08–10.60)	0.87 (0.78–1.02)	10.13 (9.59–10.54)
		8.87 (4.93–12.57)	27.32 (27.19–27.50)	8.65 (8.05–9.50)	2.35 (1.54–3.80)	9.17 (7.75–10.35)
	D3	11.86 (7.42–17.83)	26.97 (26.79–27.20)	9.69 (8.11–10.50)	0.82 (0.75–0.90)	10.08 (9.59–10.67)
		8.70 (4.83–12.37)	27.44 (27.31–27.62)	8.74 (8.07–9.37)	1.80 (1.33–2.66)	9.19 (7.86–10.34)
Sum21	A4	23.17 (21.98–24.27)	25.62 (25.14–26.20)	7.80 (7.51–8.02)	1.56 (1.20–2.15)	7.87 (5.88–9.84)
		20.55 (18.03–23.16)	26.77 (26.41–27.16)	7.36 (7.23–7.44)	3.50 (1.05–3.51)	2.60 (1.05–3.51)
(n=5)	B3	23.48 (22.36–24.77)	26.12 (25.30–26.60)	7.98 (7.90–8.04)	1.40 (1.16–1.69)	9.10 (7.99–10.85)
		20.28 (18.54–22.72)	26.98 (26.68–27.40)	7.42 (7.32–7.53)	3.07 (1.43–5.43)	3.37 (2.04–5.58)
	C2	22.93 (21.45–24.16)	26.62 (25.90–26.80)	7.90 (7.85–7.93)	1.36 (0.80–1.99)	7.80 (7.38–8.22)
		19.54 (16.38–22.50)	27.38 (27.10–27.66)	7.51 (7.45–7.58)	3.03 (1.69–4.12)	3.96 (3.23–5.25)
	D3	23.38 (22.14–24.77)	26.58 (26.00–27.00)	7.96 (7.92–8.01)	1.41 (0.96–1.94)	8.58 (7.95–9.17)
		19.30 (16.76–21.99)	27.64 (27.48–27.82)	7.51 (7.43–7.59)	5.85 (1.82–9.33)	3.92 (2.96–4.75)
Fall21	A4	20.92	25.75	7.87	1.02	6.90
		21.21	25.91	7.81	1.77	6.29
(n=1)	B3	21.18	26.50	7.84	2.16	6.55
		21.24	26.46	7.83	2.58	6.38
	C2	21.40	26.90	7.84	0.98	6.63
		21.46	26.89	7.84	2.08	6.34
	D3	22.71	26.50	7.80	0.40	6.78
		21.99	27.71	7.53	4.56	3.67

positively correlated with pH ($r=0.63$, $p=0.01$; $r=0.78$, $p=0.01$; Tables S3a, b). During 2021, hypoxia was more severe (lower DO) and covered a larger area than 2020. In 2020, bottom-water hypoxia was recorded on 20-Jul at stations A4 (2.16 mg DO l^{-1}) and B3 (2.88 mg DO l^{-1}) and remained hypoxic until recovery (DO concentrations reaching > 3.00 mg l^{-1}) was observed on 1-Sep. Although stations C2 and D3 were not categorized as hypoxic, DO was only 3.13 and 3.01 mg l^{-1} at C2 and D3, respectively, on 12-Aug (Tables 1, S2; Fig. 2). In 2021, A4 became severely hypoxic (near-anoxia) on 3-Aug (1.05 mg l^{-1}), recovering by 31-Aug. B3 was hypoxic on 3-Aug (2.54 mg l^{-1}), but recovered slightly later than A4 during Sep. Like 2020, C2 did not become hypoxic during 2021, though D3 did briefly on 16-Aug (2.96 mg l^{-1}) before recovering by 31-Aug (Tables 1, S2; Fig. 3).

Precipitation

The year 2020 was generally drier in LIS than 2021 (Table 2). Although there was considerable spatial

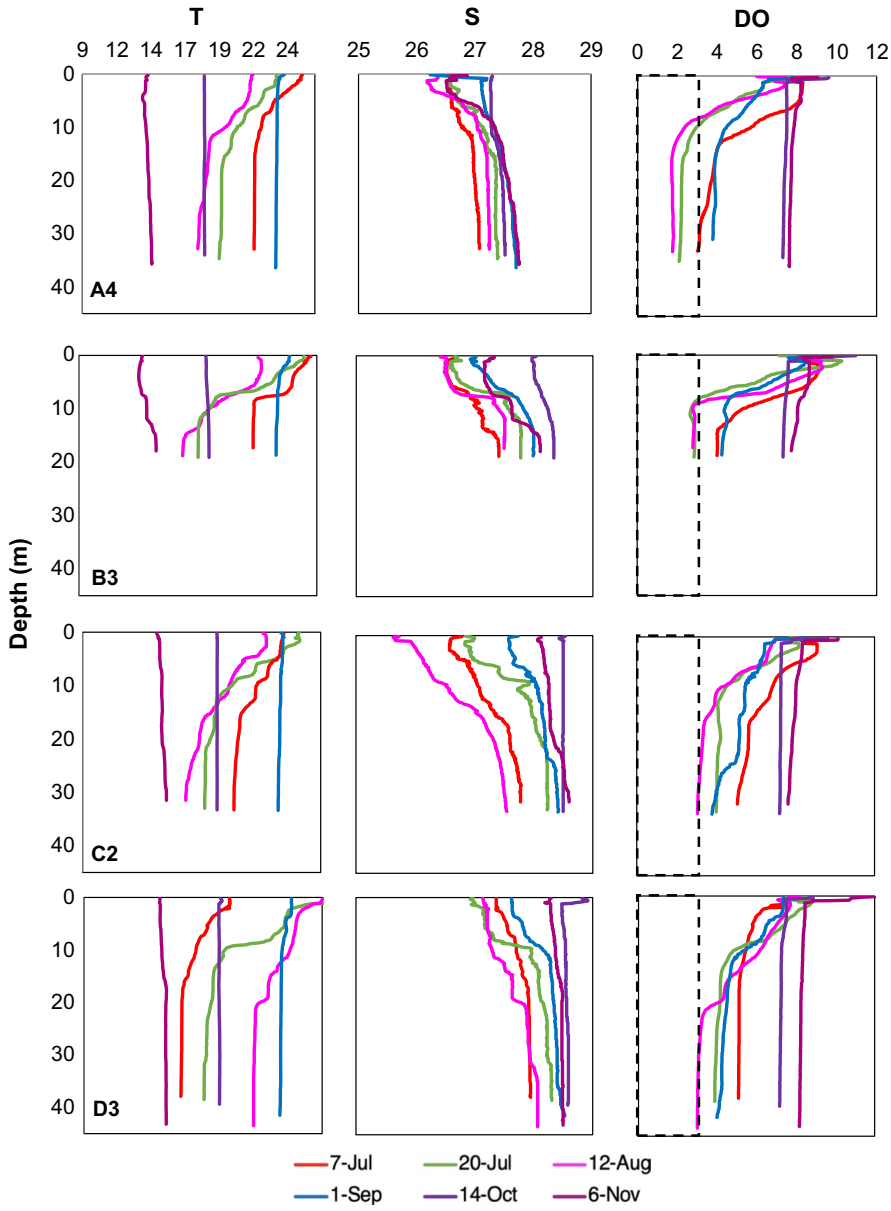

Fig. 2 Depth profiles (m) for stations A4, B3, C2, and D3 depicting water column temperature (T; °C), salinity (S; psu), and dissolved oxygen (DO; mg l^{-1}) during 2020. Measurements span sampling dates 7-Jul through 6-Nov to encompass pre-, during, and post-hypoxia timeframes. Black dashed-line boxes indicate DO measurements ≤ 3.0 mg l^{-1} (hypoxia)

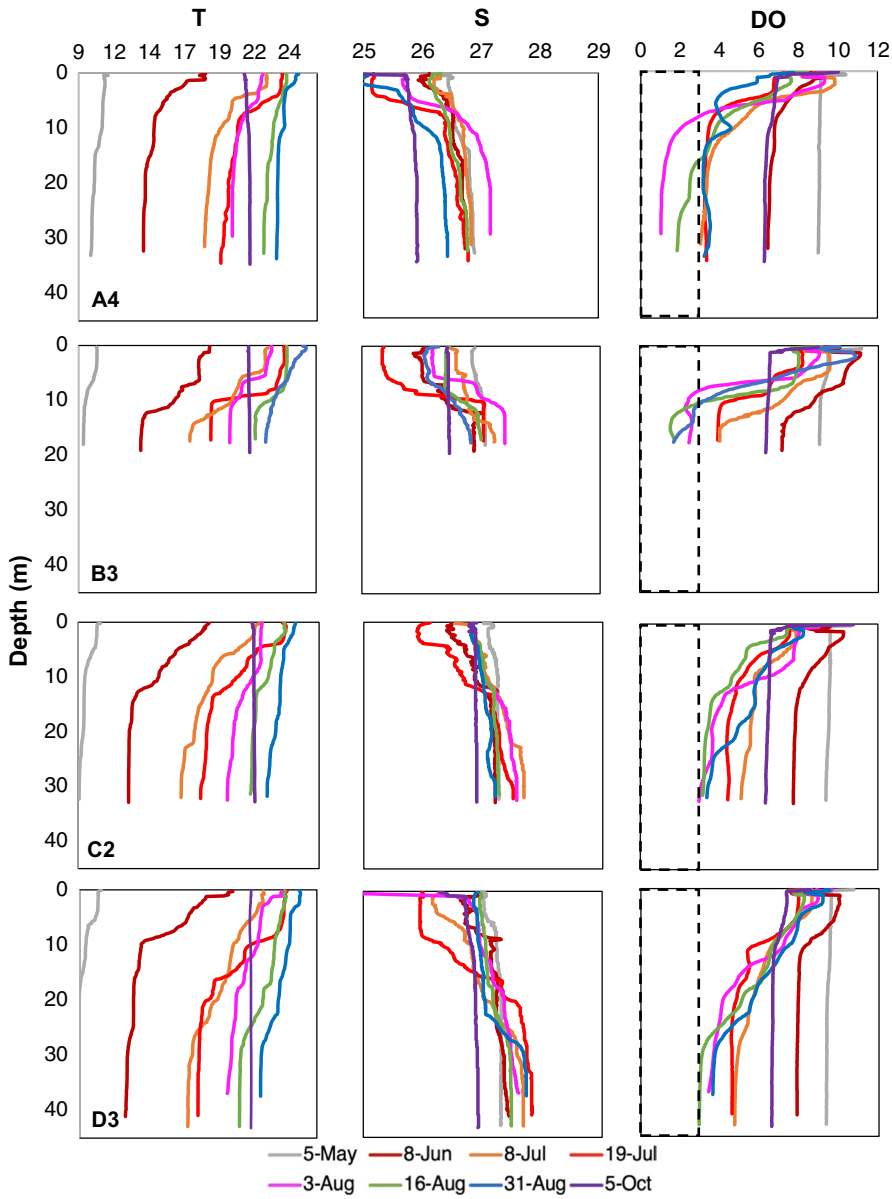

Fig. 3 Depth profiles (m) for stations A4, B3, C2, and D3 depicting water column temperature (T; °C), salinity (S; psu), and dissolved oxygen (DO; mg l^{-1}) during 2021. Measurements span sampling dates 5-May through 5-Oct to encompass pre-, during, and post-hypoxia timeframes. Black dashed-line boxes indicate DO measurements ≤ 3.0 mg l^{-1} (hypoxia)

variability in precipitation among stations for any given time interval, cumulative 7-day precipitation in 2020 was highest on 7-Jul, with a mean (SD) of 47.67 (15.54) mm and lowest on 20-Jul at 6.86 (7.48) mm. During 2021, cumulative 7-day precipitation was greatest on 8-Jul with 93.39 (23.13) mm across stations. By comparison, 10-Mar had no measurable precipitation (Table 2). Hurricane Ida made landfall in the NY region on 1-Sep 2021 with a record breaking 82.30 mm of precipitation within 1 h (Iowa State University 2022).

Dissolved inorganic nutrients

Mean $n = 3$ (SE) DIN and DIP concentrations followed a general west–east gradient with highest concentrations in the west at both depths. During 2020, mean surface AmN concentrations remained < 3.00 µM for most of the summer before increasing during fall, with the exception of D3 on 12-Aug, which was 3.40 (0.52) µM (Fig. S1a). In 2021, AmN remained < 1.00 µM, apart from A4 and B3, which exceeded 4.00 µM on 5-May (Fig. S1d).

Table 2 Cumulative daily precipitation (mm) for 7-days prior to and including each sampling date. Values are grouped as National Oceanic and Atmospheric Administration's (NOAA) weather station and their closest WLIS sampling station(s) (A4 and B3, C2, and D3). Data are from the NOAA Climate Data Online Tool (https://www.weather.gov/wrh/Climate?wfo=okx)

Sampling Date	7 day cumulative precipitation (mm)		
	A4 & B3 Port Washington 0.8 N	C2 Darien 2.4 NW	D3 Darien 1.8 ENE
7-Jul 20	29.72	56.64	56.64
20-Jul 20	12.95	9.40	9.40
12-Aug 20	15.49	2.54	2.54
1-Sep 20	14.99	8.38	8.38
14-Oct 20	34.80	30.73	30.73
6-Nov 20	23.62	16.26	16.26
10-Mar 21	0.00	0.00	0.00
7-Apr 21	12.95	11.43	11.43
5-May 21	16.51	28.96	28.19
8-Jun 21	14.48	8.89	8.64
8-Jul 21	117.09	70.87	92.20
19-Jul 21	9.91	5.59	6.60
3-Aug 21	11.43	30.99	13.21
16-Aug 21	13.21	16.76	18.80
31-Aug 21	9.91	2.54	2.29
5-Oct 21	5.08	10.92	16.51

Surface AmN was significantly and negatively correlated with both bacterial abundances at all stations (Pearson's, $r=-0.54$, $p=0.05$; Table S3a) and DO at stations A4 and B3 pooled ($r=-0.63$, $p=0.01$; Table S3c) throughout the study. During 2020, bottom AmN concentrations were highest early summer before decreasing to < 2.00 µM at all stations on 1-Sep then increasing throughout fall. During 2021, AmN increased throughout spring, reaching maxima ranging 2.20 (0.13) at D3–6.37 (0.15) µM at A4 on 8-Jun, before decreasing to < 2.00 µM from 19-Jul onwards at all stations (Figs. 4a, 5a).

During 2020, mean surface N + N concentrations remained < 2.00 µM before increasing from 1-Sep and into fall. During 2021, mean N + N concentrations remained < 2.00 µM, apart from A4 on 19-Jul, which was 5.90 (0.12) µM before generally increasing into fall (Figs. S1a, d). Like AmN, surface N + N was negatively and significantly correlated with DO at both A4 and B3 pooled (Pearson's, $r=-0.63$, $p=0.01$; Table S3c) and C2 and D3 pooled ($r=-0.51$, $p=0.05$; Table S3d) throughout the study. During 2020, bottom N + N concentrations remained < 2.00 µM during most of the summer before increasing during hypoxia and post-hypoxia (1-Sep). Similarly, 2021 N + N concentrations remained < 2.00 µM until 8-Jul, then increased throughout and post-hypoxia, though N + N 5-Oct maxima ranged 8.23 (0.06) at D3–27.69 (0.29) µM at A4 (Figs. 4a, 5a).

Overall, a clear switch between dominant DIN forms (AmN to N + N) during hypoxia occurred both years, particularly in bottom waters (Figs. 4a, 5a). At bottom depths and during high AmN, N + N concentrations were minimal. AmN concentrations were highest during Jul 2020, ranging 3.47 (0.11) µM at D3–5.07 (0.16) µM at B3 before declining to < 2.00 µM for the remaining hypoxia season (Fig. 4a). During this timeframe, N + N concentrations ranged 0.89 (0.07) µM at A4–1.31 (0.07) µM at B3 during hypoxia onset (20-Jul) before rising to 3.57 (0.03) at D3–5.53 (0.35) µM at B3 by the end of hypoxia (1-Sep) (Fig. 4a). This trend of opposing DIN concentrations was more prominent during 2021, when AmN concentrations increased throughout spring, reaching 2.18 (0.13) µM at D3–6.37 (0.15) µM at A4 on 8-Jun before decreasing to < 1.00 µM throughout hypoxia (Fig. 5a). During spring and early summer, N + N concentrations remained < 0.50 µM until hypoxia onset when concentrations increased to 1.11 (0.02) µM at A4–2.31 (0.04) µM at C2 on 3-Aug. Levels continued to increase throughout and post-hypoxia, reaching 8.23 (0.06) µM at D3–27.69 (0.29) µM at A4 on 5-Oct (Fig. 5a). At the most-hypoxic station (A4), bacterial abundances were not only positively and significantly correlated to AmN (Pearson's, $r=0.57$, $p=0.03$), they also had similar concentration trends throughout the study (Figs. 4c, 5c; Table S3k), as evidence of tight coupling.

Concentrations of PO_4^{3-} generally increased during both years. During 2020, surface PO_4^{3-} concentrations rose throughout summer, with all stations > 1.00 µM beginning 12-Aug then reaching maximum concentrations in the fall. During 2021, PO_4^{3-} concentrations were minimal (< 1.00 µM) on 19-Jul before increasing throughout the summer (Figs. S1b, e). Bottom depth PO_4^{3-} concentrations primarily remained < 1.00 µM before increasing to > 1.00 µM beginning 20-Jul 2020 and 19- Jul 2021, then remaining > 2.00 µM during hypoxia (Figs. 4b, 5b). Throughout the study, PO_4^{3-} concentrations

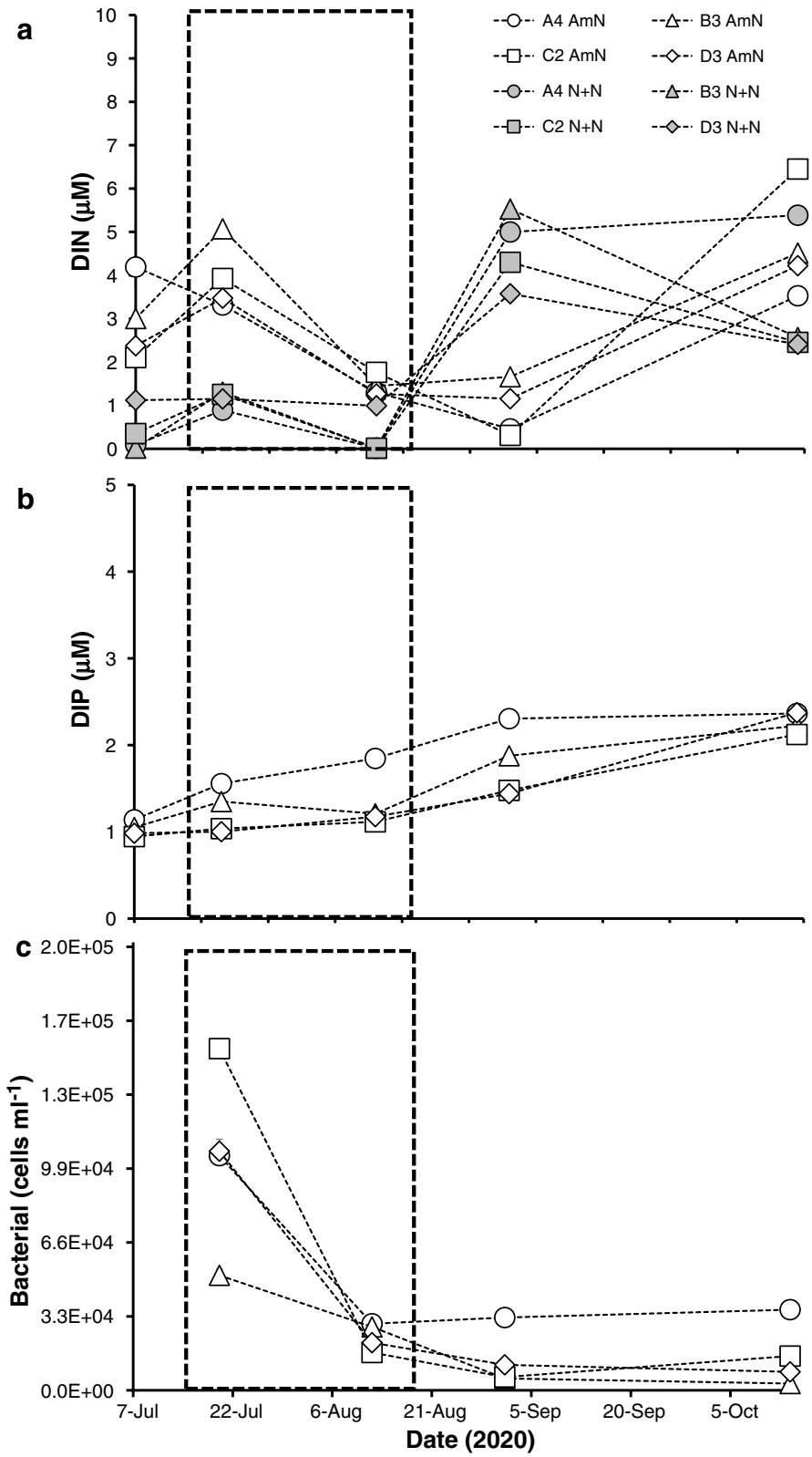

Fig. 4 Mean ($n=3$) (SE) bottom depth concentrations (µM) of $NH_4^+ + NH_3$ (AmN) and $NO_2^- + NO_3^-$ (N + N) (**a**); PO_4^{3-} (DIP) (**b**); and bacterial abundances (cells ml^{-1}) (**c**) at stations A4, B3, C2, and D3 during 2020. Symbols for all figures represent the same stations, with A4 shown by circle marker, B3 by triangle, C2 by square, and D3 by diamond. Black dashed-line boxes indicate DO measurements ≤ 3.0 mg l^{-1} (hypoxia)

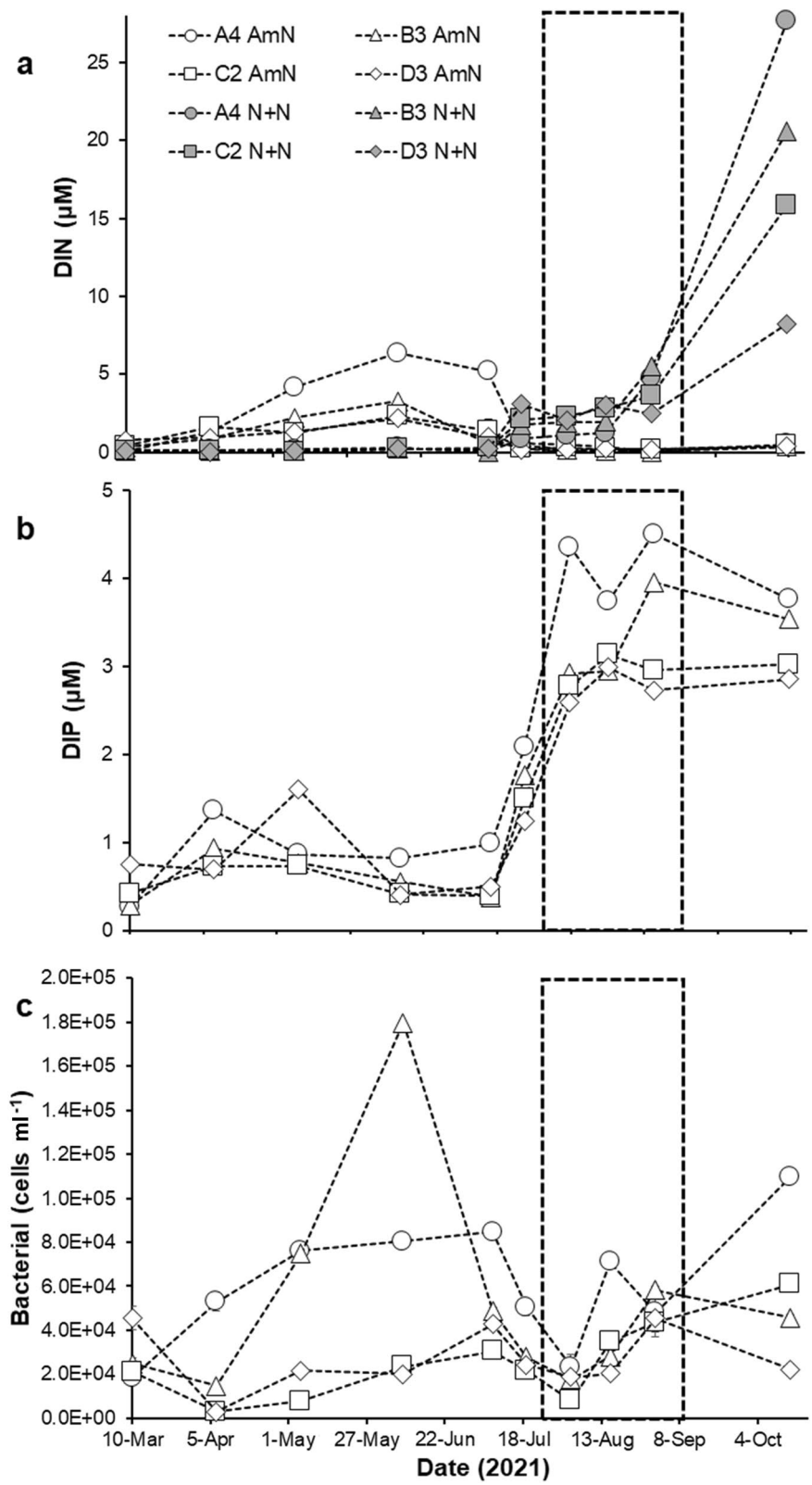

Fig. 5 Mean ($n = 3$) (SE) bottom depth concentrations (µM) of $NH_4^+ + NH_3$ (AmN) and $NO_2^- + NO_3^-$ (N + N) (**a**); PO_4^{3-} (DIP) (**b**); and bacterial abundances (cells ml^{-1}) (**c**). Symbols for all figures represent the same stations, with A4 shown by circle marker, B3 by triangle, C2 by square, and D3 by diamond. Black dashed-line boxes indicate DO measurements ≤ 3.0 mg l^{-1} (hypoxia)

were negatively and significantly correlated to DO at all stations (except D3) as A4 ($r=-0.69$, $p=0.01$; $r=-0.60$, $p=0.02$), B3 ($r=-0.75$, $p=0.00$; $r=-0.57$, $p=0.03$), and C2 ($r=-0.56$, $p=0.04$; $r=-0.59$, $p=0.03$) at both surface and bottom depths, respectively (Tables S3g-m).

Dissolved organic matter

Consistent with trends of increasing DO eastward, concentrations of mean $n=3$ (SE) DOM were generally greatest in the western-most portion of WLIS, with surface DOM concentrations ranging 151.70 (1.81) at C2–1,304.47 (105.33) µM at B3 (Fig. 6a) and mean bottom depth DOM concentrations ranging 148.59 (0.75)–1099.71 (29.27) µM, both at A4 (Fig. 6b). DOC comprised the largest proportion of the DOM pool for all samples with the exceptions of 5-Oct at stations A4 and B3 for both depths and on 31-Aug at stations C2 and D3, when DON was the dominant proportion of DOM (Fig. 6). DOP was the smallest DOM proportion in all samples.

Of individual DOM pools, mean $n=3$ (SE) DON concentrations ranged 0.00 (0.00)–1,029.08 (182.00) and 0.00 (0.00)–747.28×10^2 (16.80) µM for surface (Fig. 6a) and bottom (Fig. 6b) depths, respectively, at all stations. For both depths, DON concentrations were lowest during early summer and highest during late summer and fall. A DON peak (> 500.00 µM) occurred at stations A4 and B3 on 5-Oct at both depths (Fig. 6). Mean $n=3$ (SE) DOP concentrations ranged 0.00 (0.00)–8.73 (2.66) and 0.00 (0.00)–2.09 (0.10) µM for surface (Fig. 6a) and bottom (Fig. 6b) depths, respectively, at all stations. For both depths, DOP concentrations were minimal throughout most of the study, with highest concentrations during summer (Fig. 6) and at station D3, followed by B3, A4, and C2. Both surface DON and DOP were negatively and significantly correlated with precipitation at stations C2 and D3 pooled (Pearson's, DON: $r=-0.53$, $p=0.04$; DOP: $r=-0.62$, $p=0.01$; Table S3d). Mean $n=2$ (SD) DOC concentrations ranged 149.03 (7.94)–417.95 (18.2) and 147.36 (0.00)–535.34 (17.01) µM for surface (Fig. 6a) and bottom (Fig. 6b) depths, respectively, at all stations. Unlike DON or DOP, levels of DOC did not follow a defined seasonal or spatial pattern. At stations A4, B3, and C2, bottom DOC concentrations were highest (> 200 µM) on 16-Aug 2021, whereas peak concentrations at D3 (1.67×10^2 (0.00) µM) were recorded on 31-Aug 2021(Fig. 6b). Bottom depth DOC was negatively and significantly correlated with DO for A4 and B3 pooled (Pearson's, $r=-0.53$, $p=0.05$; Table S3e), coincident with greatest hypoxia severity westward.

Bacterial abundances

Mean $n=3$ (SE) bacterial abundances were generally higher in surface than bottom depths. Surface bacterial abundances ranged 4.03×10^3 (1.53×10^3)–2.28×10^5 (1.91×10^4) cells ml^{-1} at all stations both years (Figs. S1c, f). In 2020, surface bacterial abundances were generally highest on the first sampling date, 20-Jul then decreased to $<1.00\times10^5$ cells ml^{-1} throughout hypoxia, and remained low post-hypoxia. The exception was A4, which reached 4.31×10^4 (5.95×10^3) cells ml^{-1} on 1-Sep (Fig. S1c). During 2021, surface bacterial abundances rose throughout spring and into early summer at all stations, before a sharp decline ($<6.00\times10^4$ cells ml^{-1}) on 3-Aug during hypoxia, before increasing again (Figs. S1c, f). Mean surface bacterial abundances were generally highest at station B3, followed by C2, A4, and D3 both years (Figs. 4c, 5c) but were not significantly different between stations A4 and B3 pooled or stations C2 and D3 (Two sample t-Tests assuming equal variances between A4 and B3 ($p=0.25$), C2 ($p=0.45$), and D3 ($p=0.10$)). However, they were negatively and significantly correlated with AmN (Pearson's, $r=-0.54$, $p=0.05$; Table S3a) across WLIS, particularly at A4 and B3 pooled ($r=-0.54$, $p=0.04$; Table S3c) as well as negatively and significantly correlated to salinity as A4 ($r=-0.55$, $p=0.03$; Table S3g) and B3 ($r=-0.76$, $p=0.00$; Table S3h) throughout the study.

Bottom depth mean ($n=3$) (SE) bacterial abundances ranged 3.02×10^3 (6.36×10^2)–1.80×10^5 (5.50×10^3) cells ml^{-1} across all stations (Figs. 4c, 5c) and followed a west–east gradient with highest concentrations in the west. In 2020, highest bottom depth abundances occurred on 20-Jul, ranging 5.13×10^4 (5.47×10^3) at B3–1.53×10^5 (7.36×10^3) cells ml^{-1} at C2. Bacterial abundances decreased during the remainder and post-hypoxia, staying $<4.00\times10^4$ cells ml^{-1} at all stations 2-Aug–14-Oct (Fig. 4c). In 2021, bacterial abundances increased throughout spring with maximum concentrations on 8-Jun for B3 of 1.80×10^5 (5.50×10^3) and 8.47×10^4 (2.18×10^4), 3.05×10^4 (2.23×10^3), and 4.27×10^4 (1.24×10^4)

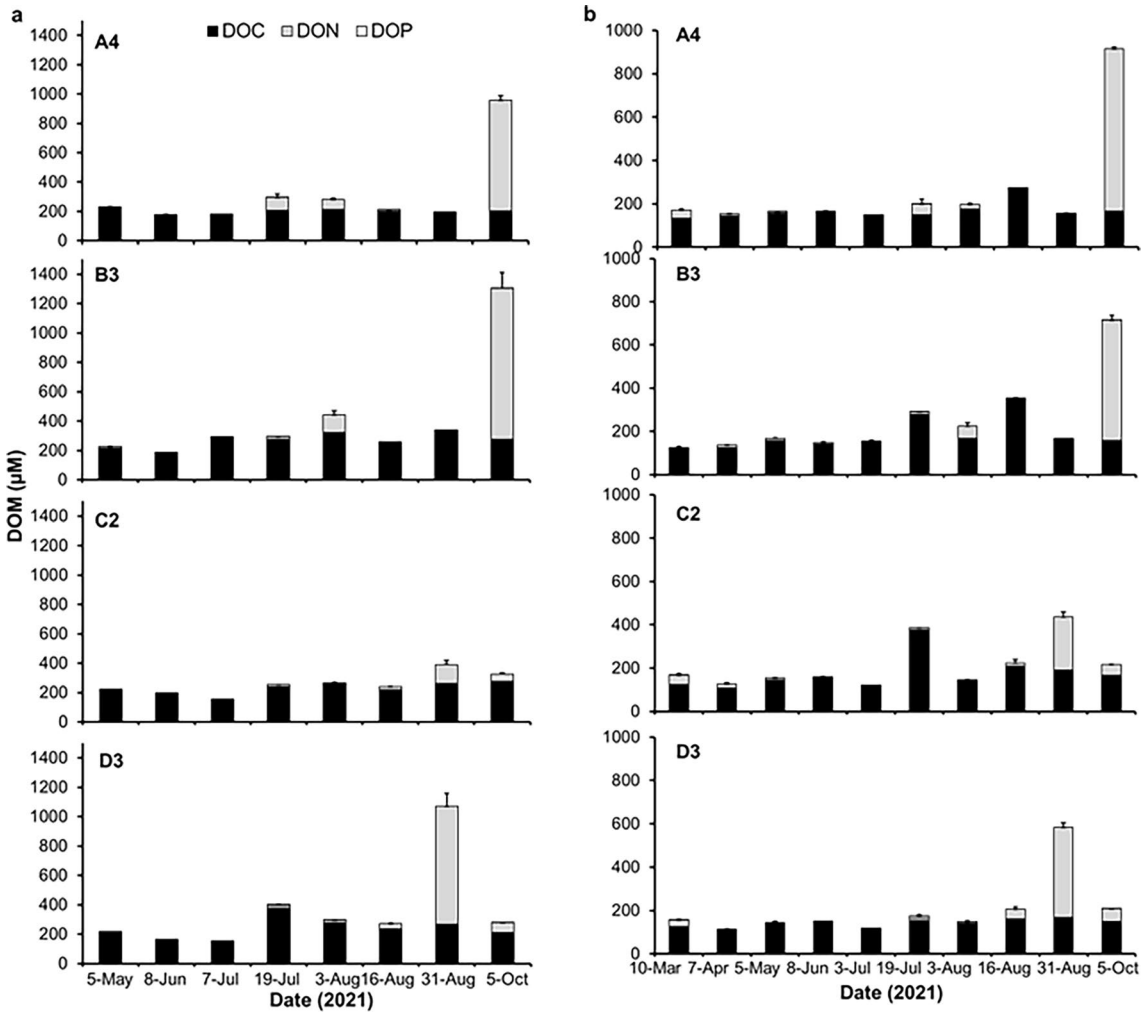

Fig. 6 Mean ($n=3$) (SE) Dissolved organic matter (DOM; μM) concentrations, during 2021 depicting individual pools of dissolved organic carbon (DOC; black), nitrogen (DON; grey), and phosphorus (DOP; white), for stations A4, B3, C2, and D3 at (**a**) surface (2 m) (**b**) and bottom (-5 m from benthos) depths. Note difference in y-axis scales between depths. Results for 10-Mar and 7-Apr at surface depths are omitted because DOC samples were not collected on those dates

cells ml^{-1} on 8-Jul at A4, C2, and D3, respectively. Bacterial abundances declined to $< 2.50 \times 10^4$ cells ml^{-1} during hypoxia onset (3-Aug) then increased through post-hypoxia (Fig. 5c), but remained significantly higher at A4 than the least-hypoxic stations C2 (Two sample t-Tests assuming equal variances, $p=0.02$) and D3 ($p=0.01$) throughout the study. Finally, during both summers, pooled bacterial abundances were negatively and significantly correlated to DON (Pearson's, $r=-0.87$, $p=0.01$; Table S3p).

Chl *a*

Mean ($n=3$) (SE) surface chl *a* ranged 1.38 (0.01)–25.8 (0.27) μg l^{-1} at all stations during both years. Chl *a* concentrations depicted clear seasonality, with highest concentrations during summers and lowest in the winter (Fig. 7). Chl *a* followed a decreasing west–east gradient, with an overall mean of 9.91 μg l^{-1} at A4, followed by B3 (9.80 μg l^{-1}), C2 (5.34 μg l^{-1}), and D3 (4.82 μg l^{-1}). Highest chl *a* concentrations coincided with phytoplankton blooms. Causative bloom taxa included euglenoids in 2020

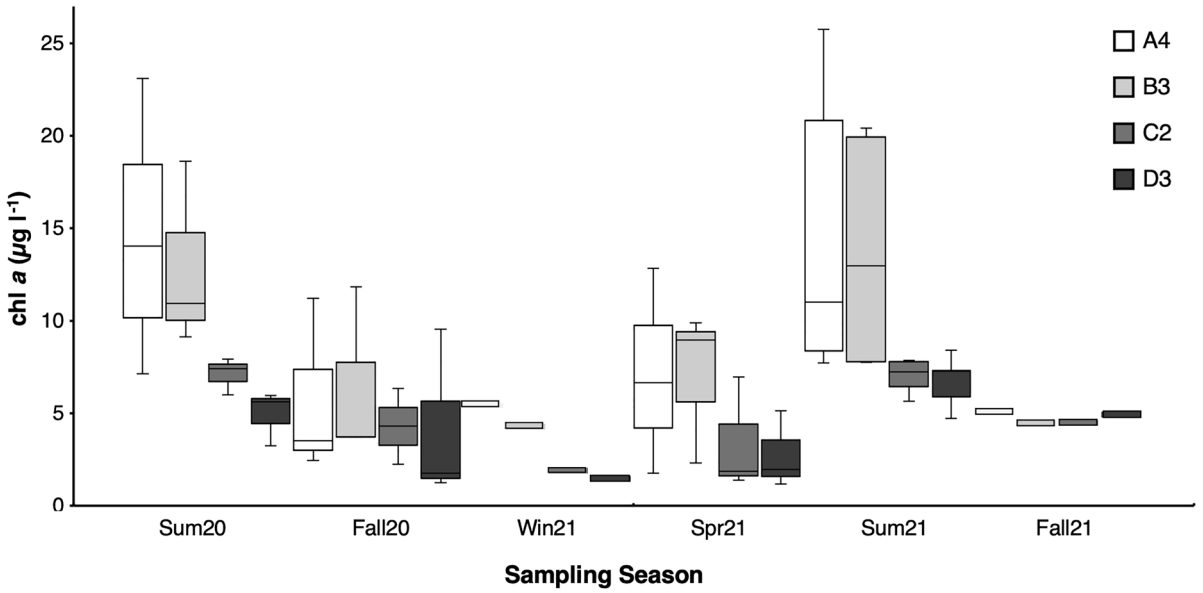

Fig. 7 Boxes represent median ($n=3$) (SE) chl *a* (µg l^{-1}) measurements for each sampling date pooled, corresponding to solar seasons (2020–2021) for stations A4, B3, C2, and D3. X-axes labels depict seasons as summer 2020 (Sum20), fall 2020 (Fall20), winter 2021 (Win21), spring 2021 (Spr21), summer 2021 (Sum21), and fall 2021 (Fall21)

as well as the diatoms *Leptocylindrus* in 2021 and *Skeletonema* during both summers (Roldan Ayala et al. In Review). Chl *a* was significantly and negatively correlated to both DIN forms: AmN (Pearson's, $r=-0.66$, $p=0.01$) and N+N ($r=-0.73$, $p=0.00$) throughout the study (Table S3a). Chl *a* at A4 and B3 pooled were negatively and significantly correlated with AmN ($r=-0.62$, $p=0.01$; Table S3c). Additionally, chl *a* at A4 and B3 pooled was positively and significantly correlated with DO ($r=0.83$, $p=0.00$; Table S3c) while chl *a* at C2 and D3 pooled was negatively and significantly correlated with DO ($r=-0.60$, $p=0.02$; Table S3d), coincident with a positive and significant correlation with bacterial abundances at D3 ($r=0.56$, $p=0.03$; Table S3j).

Discussion

This study showed that the onset of summer bottom-water hypoxia in WLIS is characterized by both a significant shift in the dominant form of DIN (AmN to N+N) and a decline in bacterial abundances. Results provide novel evidence that ammonia oxidation ($NH_3 \rightarrow NO_2^-$) is enhanced by hypoxia in WLIS and therefore likely a key reaction during nitrification ($2NH_3$ (or NH_4^+) $+ 3O_2 \rightarrow NO_2^- + 2H_2O + 2H^+ \rightarrow NO_3^-$) within the water column, contributing to subsequent N+N increases. Similarly, bacterial abundances were closely associated with DO levels, as they declined from pre- to the onset of hypoxia, then rose post-hypoxia, perhaps indicating that nitrification rates increased as oxic conditions were restored. The significant negative correlation between DO and bottom water DOC at the most severely hypoxic stations (A4 and B3) was consistent with increased BOD in response to greater bioavailability of organic C-rich OM, a major driver of hypoxia onset in WLIS.

Most biogeochemical (N and P) and ecological (chl *a* and bottom bacterial abundances) metrics followed a declining west–east gradient throughout the study, except for DOC and surface bacterial abundances. Western-most stations A4 and B3, which were closest to NYC, exhibited greater hypoxia severity (lowest DO levels) and coverage (longest duration and largest area) than stations C2 and D3, consistent with historical trends of increasing DO levels eastward (Parker and O'Reilly 1991; Lee and Lwiza 2008; CTDEEP 2019, 2020). Anoxia was not detected during the study. Physical water quality followed similar patterns with relatively higher temperatures, and lower salinity

and pH at both depths in the west. These findings support previous observations of the western, urban locations having higher N levels, chl *a*, temperatures, and lower salinities than either CLIS or ELIS (Taylor et al. 2003; Lee and Lwiza 2005; Gobler et al. 2006; CTDEEP 2019; Vlahos et al. 2020).

Water column stratification coincided with hypoxia in WLIS both summers, evidenced by the development of Jul 2020 and Jun 2021 thermoclines and a Jul halocline both years. The water column remained stratified at all stations until Sep. Since water column stratification has been associated with LIS oxygen minima (Jensen et al. 1990; Lee and Lwiza 2008), this study confirms that physical processes directly influenced hypoxia severity and coverage. Physical processes have intensified hypoxia along other coasts, such as by constraining DOM-rich waters nearshore that increase heterotrophic oxygen demand in Myrtle Beach, SC (Sanger et al. 2012) and by strong currents of subarctic water into the California Current System reducing DO levels in OR (Grantham et al. 2004).

The transition between bottom water DIN forms (AmN to N + N) from pre-hypoxia to hypoxia, respectively, indicates that low DO conditions favor ammonia oxidation in WLIS. Ammonia oxidation and potentially enhanced rates of nitrification likely affected N-cycling within WLIS, since ammonia oxidation is often the first and rate-limiting step of nitrification (Lehtovirta-Morley 2018). Supporting evidence comes from 16S sequence analyses (Santoferrara et al. 2022), which showed that proportions of ammonia-oxidizing archaea (AOA) were elevated during maximum WLIS hypoxia in 2019 (DO 0.90–3.10 mg l^{-1}; CTDEEP 2019). While the present study did not entail parallel 16S sequencing, combining field metrics with genomic analyses would be highly valuable for future hypoxia research. AOA have also been significantly correlated to abundances of ammonia-oxidizing bacteria (AOB), with potential nitrification rates accelerating as AOA abundances increase (Caffrey et al. 2007). Both AOA and AOB have physiological mechanisms that enable them to tolerate hypoxic conditions (Stein 2019). Since nitrification can occur in minimally oxic conditions and anoxia was not detected during this study, increased nitrification likely occurred during and through post-hypoxia, when bottom water DO recovered (> 3.00 mg l^{-1}). The resultant N + N products in bottom waters could then be lost by anaerobic ammonia oxidation in sediments (anammox; $NH_4^+ + NO_2^- \rightarrow N_2 + 2H_2O$) or by denitrification ($NO_3^- \rightarrow NO_2^- \rightarrow NO + N_2O \rightarrow N_2O + N_2$), which is often the dominant loss pathway for fixed N in estuaries (Mosier and Francis 2010; Lehtovirta-Morley 2018). Similar patterns in DIN forms spanning hypoxia, particularly increased NO_2^- concentrations, occur in other U.S. estuaries, with mid-summer peaks in AOA correlating with NO_2^- accumulation, increased temperatures (Hollibaugh et al. 2014; Schaefer and Hollibaugh 2017), and decreases in NH_4^+ concentrations (Hollibaugh et al. 2014). Enrichment of ammonia-oxidizing genes and transcripts have also been found in deeper, more oxygen-depleted layers. For example, in the Louisiana Shelf, NO_2^- accumulation commonly occurs under low oxygen conditions (Bristow et al. 2015). Combined, these studies suggest that hypoxia substantially impacts N-cycling pathways in estuarine bottom waters.

Another explanation for the switch in dominant DIN form during hypoxia could be lower N-mineralization (organic N $\rightarrow NH_3 \rightarrow NH_4^+$) by heterotrophic bacteria. As DO concentrations decrease, sedimentary N mineralization may be reduced (Neubacher et al. 2011), resulting in a decline in NH_4^+ concentrations. In this study, while AmN levels decreased during hypoxia, they were never depleted, indicating a reduction of DOM decomposition rates due to feedbacks from low DO conditions. A low DO environment could also slow nitrification rates (Henriksen and Kemp 1986; Caffrey et al. 2007), but if N mineralization is more suppressed than nitrification, then a decrease in AmN concentrations would occur during N + N production. This underscores the necessity to measure nitrification rates in WLIS in the future.

PO_4^{3-} concentrations increased during hypoxia both study years, indicating that DIP was not limited in surface waters. Available P can intensify phytoplankton or bacterial uptake of dissolved PO_4^{3-} (and DOP) from the water column, increasing chl *a* (Dyhrman and Ruttenberg 2006; Paytan and McLaughlin 2007). In bottom-waters, organic P can be mineralized (DOP $\rightarrow PO_4^{3-}$) via degradation of OM (Lin et al. 2016), which could have enhanced PO_4^{3-} concentrations in the late summers. Another source of PO_4^{3-} could be the biological accumulation of P in sludge (sewage byproduct), which is primarily conducted by P accumulating organisms in environments that cycle between aerobic and anaerobic

states (Tarayre et al. 2016) and release PO_4^{3-} under anaerobic conditions. The significant negative correlation between DO and PO_4^{3-} has been observed in LIS previously (Ballestero et al. 2018). In this study, it coincided with the significant and positive correlation between DO and pH, suggesting that the more acidic environment influenced conversions between other inorganic P forms to PO_4^{3-}.

At bottom depths, DOM was linked to microbial processes across WLIS as highest DOM levels were at the most hypoxic stations, indicating that DOM was a primary driver of hypoxia. Within the DOM pool, DOC levels were generally within range of previous DOC measurements (Jul–Oct 1992–1993) of 223–378 and 168–309 µM C (no error terms reported) in surface and bottom depths, respectively, with maximum concentrations towards the end of the observational period (Anderson and Taylor 2001) as well as lower mean (SD) DOC concentrations of 175 (16) µM l^{-1} and 158 (25) µM l^{-1} at A4 surface and bottom depths, respectively, beginning 2008 (Whitney and Vlahos 2017), with higher concentrations typically in summers. In this study, the highest DOM levels closest to NYC and at the most hypoxic stations was consistent with urbanized regions contributing greater amounts of labile DOM that enhance microbial degradation rates (Supino 2020). The negative and significant correlation between DON and bacterial abundances during the summer indicated microbial uptake of DON. Finally, the peak DOM and DON levels at both depths for the western-most stations on 5-Oct of 2021 coincided with abnormally high *Enterococcus* (565 count 100 ml^{-1}) levels that led to a beach advisory (Riverkeeper 2022), evidence of a mass combined sewage overflow (CSO) event.

Considering that phytoplankton provide DOC to bacteria post-carbon fixation (Bertilsson and Jones 2003; Goñi et al. 2003; Azam and Malfatti 2007; Findlay and Parr 2017), and chl *a* and DOM were typically highest further west, it is possible that phytoplankton contributed DOC that enriched bottom depth DOM concentrations. In Long Island's Great South Bay, where both DOM and chl *a* can be significantly elevated, chl *a* has been positively (temporally and spatially) associated with both DON and DOC such that chl *a* and DOC concentrations were highly and significantly correlated (Lonsdale et al. 2006). While DOC was not significantly correlated to chl *a* in this study, DON levels decreased eastward in tandem with chl *a*.

Trends in bacterial abundances (maxima pre-hypoxia followed by decreases during hypoxia) were similar to previous LIS studies, when bottom depth bacterial biomass peaked late Jul/early Aug before decreasing (Anderson and Taylor 2001; Liu et al. 2015). Reductions in bacterial abundances during DO minima occur in other northeastern U.S. hypoxic waterbodies (Weinke and Biddanda 2018), suggesting processes observed in LIS may be more common than previously thought. This pattern could be attributed to succession in dominant microbes. For example, in WLIS during 2019, proportions of the AOA *Nitrosopumilus maritimus* were greater during hypoxia than pre-hypoxia (Santoferrara et al. 2022). This species is typically 0.17–0.22 µm in diameter and 0.50–0.90 µm in length (Könneke et al. 2005), which is smaller than the 0.20–2.00 µm size range of bacteria quantified during this study. *N. maritimus* cells < 0.20 µm would have been excluded from analysis, leading to an under-estimate of microbial abundances. Conversely, since nitrifying bacteria are prone to dense aggregation (Gieseke et al. 2001), and bottom-water turbidity increased during summers, particles > 2.00 µm containing AOB would have been excluded. Since ammonia oxidation followed by nitrite oxidation ($NO_2^- \rightarrow NO_3^-$) is primarily catalyzed by nitrite-oxidizing bacteria (NOB), the slow autumnal recovery of bacterial abundances towards the end of hypoxia along with increasing N + N concentrations could have been due to the extended growth rates and generation times of aerobic autotrophic microbes during NO_2^- oxidation (Wijffels et al. 1996; Dworkin and Gutnick 2012), with some close relatives of NOB completing nitrification (Jun and Wenfeng 2009; Daims et al. 2016). The spike in N + N on 5-Oct 2021 was likely excess NO_3^- released during the CSO event and/or a general trapping of N in the western-most portion of the estuary.

Chl *a* concentrations portrayed both seasonality (highest measurements in the summer) and a declining west–east gradient. Similarly, chl *a* during Jan–Aug 2019, depicted similar maximum (2 m depth) measurements with concentrations of 23.1 µg l^{-1} at A4, ~ 16.0 µg l^{-1} at B3, and ~ 11.0 µg l^{-1} at D3 (CTDEEP 2019). The significant negative correlation between chl *a* and DIN forms in surface depths both study years indicated DIN uptake by

phytoplankton, aligning with phytoplankton biomass enhanced by DIN availability/concentrations (Gobler et al. 2006; Glibert et al. 2018; Sitta et al. 2018 and others). Additionally, the significant negative correlations between surface DOP and chl *a* during summers indicated DOP uptake by phytoplankton. Flagellates (euglenoids and *Prorocentrum* sp.) and diatom (2021) blooms were detected both summers in WLIS (Roldan Ayala et al. In Review), coincident with elevated chl *a*. The negative and significant correlations between surface chl *a* and DO at A4 and B3, where chl *a* was highest, suggests that photosynthesis paralleled BOD oscillations (Anderson and Taylor 2001). The positive and significant correlations between chl *a* and bacterial abundances at D3 may be due to microbial-phytoplankton synergies or another factor, such as temperature inducing microbial growth. Future studies should explore the extent and nature of phytoplankton-bacterial biogeochemical relationships within LIS, particularly related to N-cycling and DOM production. Surface-bottom coupling may occur, with DIN fueling phytoplankton that subsequently enhances DOM, though the extent to which this occurs and/or influences hypoxia relative to urban DOM and N sources needs to be explored thoroughly.

Warming of waterbodies via climate change is predicted to decrease oxygen solubility and increase respiration both in WLIS (Whitney and Vlahos 2021) and globally (Altieri and Gedan 2014; Breitburg et al. 2018), consistent with a worldwide increase in hypoxia severity (Carstensen et al. 2014; Rabalais et al. 2015; Breitburg et al. 2018; Chan et al. 2019). In LIS broadly, warming-induced reductions in oxygen solubility may erode 35% of oxygen gains by 2099, as temperatures are increasing at a rate of 0.08 ± 0.03 °C per year, which is faster than the global average (0.10 °C per decade) (Staniec and Vlahos 2017). Climate change is predicted to impact similarly eutrophic hypoxic estuaries, such as Chesapeake Bay, where lower oxygen solubility could account for ~ 50% of the reduction in bottom-water oxygen and 10–30% of the expansion in hypoxic/anoxic volumes by the mid-twenty-first century (Ni et al. 2019). Moreover, sea level rise and heightened winter-spring runoff may strengthen stratification/weaken vertical exchange, also contributing to hypoxia (Jensen et al. 1990; Altieri and Gedan 2014; Rabalais et al. 2010; Du et al. 2018; Ni et al. 2019). While potentially inducing water-column mixing, greater storm precipitation may accelerate riverine nutrient (N) loading that fuels microbial activity and intensifies hypoxia (Rabalais et al. 2010; Sinha et al. 2017; Whitney and Vlahos 2021). N budgets in WLIS are sensitive to the timing of wastewater discharge through the East River tidal straight, though NH_4^+ has a net import to LIS broadly (Vlahos et al. 2020). The extent to which the many rivers feeding LIS contribute specific DIN forms to LIS is not well-known. This is a substantial management concern because N load reductions beyond the current TMDL may need to be considered to offset future oxygen solubility declines.

Results from this study indicate that the biogeochemical feedbacks between WLIS water column and benthic processes are tightly linked to hypoxia. Benthic nitrification and denitrification are primary drivers of sediment nitrous oxide (N_2O) production (Meyer et al. 2008; Barnes and Upstill-Goddard 2018; Foster and Fulweiler 2019; Yang et al. 2022), but sediment releases of the potent greenhouse gases N_2O and methane (CH_4) are controlled by OM availability (Mazur et al. 2021), specifically anoxic sediments during high OM loading that accelerate C remineralization via methanogenesis (Gelesh et al. 2016). LIS sediments are a source of N_2O ($8.63 + 3.18$ nmol m^{-2} h^{-1}) and CH_4 ($23.80 + 18.05$ nmol m^{-2} h^{-1}; Mazur et al. 2021). Continued hypoxia risks catalyzing biogeochemical processes that release both N_2O and CH_4 while diminishing sediment consumption of N_2O (Naqvi et al. 2010; Voss et al. 2013; Foster and Fulweiler 2019; Stein 2019). Thus, the combination of ammonia oxidation followed by coupled nitrification–denitrification may accelerate both greenhouse gas production and N loss to the atmosphere via N_2 (Rich et al. 2008; Nicholls and Timmer 2009; Mosier and Francis 2010; Lehtovirta-Morley 2018). Further studies are needed to quantify these processes within LIS.

This study provides novel insights to feedbacks between major biogeochemical (N and C) cycles, bacterial populations, and hypoxia in WLIS. DON and DOC were linked with bottom water microbial abundances and summer hypoxia. Additionally, the switch in DIN from AmN to N + N during hypoxia coincident with bacterial abundance trends in bottom-waters spanning hypoxia both study years suggest that ammonia oxidation, or alternatively imbalanced N-mineralization and nitrification rates, generates NO_2^- and NO_3^- during and

post-hypoxia. Elevated bottom N + N may regulate the subsequent loss of N via denitrification from LIS, though additional studies that quantify denitrification, nitrification, and N-mineralization rates are needed. With climate change induced warming of waters predicted to exacerbate hypoxia, these biogeochemical processes may be accelerated, underscoring the need to reassess N management strategies within WLIS as well as urbanized estuaries broadly.

Acknowledgements We gratefully thank the crew of the *R/V John Dempsey* with the Connecticut Department of Energy and Environmental Protection for help collecting water samples during their LIS surveys. Big thank you to current and previous Greenfield lab members Dr. Sílvia Anglès and Maximillian Brown, Tzortziou Lab members Dr. Jonathan Sherman, Dr. Minsun Lee, Alana Menendez and Kyle Turner– City College of New York, and the Goes Lab (Lamont-Doherty Earth Observatory). Additional thanks to the ConEdison STEEM Graduate Scholarship, the Queens College Masters Scholarship, Coastal and Estuarine Research Federation Rising Tides Program, and interns Gabriella Rodriguez (2022 Velay Women Scholars Research Fellowship) and Anne Zatz (2021 CUNY Summer Undergraduate Research Program).

Author contributions All authors contributed to the study conception and design. GEH (a) conducted the bacterial sample processing and analyses, (b) evaluated chlorophyll levels, (c) oversaw nutrient analyses, (d) conducted statistical analyses, generated figures, and was the primary author of the text. JE assisted in sample collection as well as 2020 nutrient and chlorophyll analyses. MA assisted in 2021 nutrient analyses, assisted in field sample collection and processing, and helped oversee DOC sample analysis. ZRA conducted phytoplankton analyses and assisted in the image analysis. MT and JG are PIs on the grant that funded the study and contributed to overall project design and sample collection. DG was the PI who oversaw this project, the primary advisor of GEH, and supervised manuscript organization and editing. All authors read and approved the final manuscript.

Funding Funding is courtesy of Environmental Protection Agency award #LI 96261317 Subaward # 82913/2/1156439, National Science Foundation awards #DEB-2039867 and #DEB-2039877, and the City University of New York (CUNY)—Advanced Science Research Center.

Data availability Water quality data, surface depth graphs, and correlation matrixes are provided as supplemental information. Additional data are archived at the CUNY Advanced Science Research Center and can be shared upon request.

Declarations

Competing interests The authors declare no competing interests.

Competing interest The authors have no relevant financial or non-financial interests to disclose.

References

Altieri AH, Gedan KB (2014) Climate change and dead zones. Glob Change Biol 21(4):1395–1406. https://doi.org/10.1111/gcb.12754

Anderson TH, Taylor GT (2001) Nutrient pulses, phytoplankton blooms, and seasonal hypoxia in the western Long Island Sound. Estuaries 24:228–243. https://doi.org/10.2307/1352947

Azam F, Malfatti F (2007) Microbial structuring of marine ecosystems. Nat Rev Microbiol 5:782–791. https://doi.org/10.1038/nrmicro1747

Ballestero H, Doiron K, Levine M, Friedman S (2018) Synthesis and analysis of historical hypoxia data in the western narrows of the Long Island Sound—Final Report. Interstate Environmental Commission NY-NJ-CT, 1–94. https://www.iec-nynjct.org/sites/default/files/2018-08/Industrial%20Economics_%20Hypoxia%20Narrows%20LIS%20Repor.pdf

Barnes J, Upstill-Goddard RC (2018) The denitrification paradox: the role of O_2 in sediment N_2O production. Estuar Coast Shelf Sci 200:270–276. https://doi.org/10.1016/j.ecss.2017.11.018

Bertilsson S, Jones JB (2003) Supply of dissolved organic matter to aquatic ecosystems: autochthonous sources. Aquatic ecosystems—interactivity of dissolved oxygen. Academic Press, San Diego, pp 3–24

Borsuk ME, Stow CA, Luettich RA, Paerl HW, Pinckney JL (2001) Modelling oxygen dynamics in an intermittently stratified estuary: estimation of process rates using field data. Estuar Coast Shelf Sci 52(1):33–49. https://doi.org/10.1006/ecss.2000.0726

Breitburg D, Levin LA, Oschlies A, Grégoire M, Chavez FP, Conley DJ, Garçon V, Gilbert D, Gutiérrez D, Isensee K, Jacinto GS, Limburg KE, Montes I, Naqvi SWA, Pitcher GC, Rabalais NN, Roman MR, Rose KA, Seibel BA, Telszewski M, Yasuhara M, Zhang J (2018) Declining oxygen in the global ocean and coastal waters. Sci 359(6371):1–11. https://doi.org/10.1126/science.aam7240

Bristow LA, Sarode N, Cartee J, Caro-Quintero A, Thamdrup B, Stewart FJ (2015) Biogeochemical and metagenomic analysis of nitrite accumulation in the Gulf of Mexico hypoxic zone. Limnol Oceanogr 60(5):1733–1750. https://doi.org/10.1002/lno.10130

Buchan A, LeCleir GR, Gulvik CA, González JM (2014) Master recyclers: features and functions of bacteria associated with phytoplankton blooms. Nat Rev Microbiol 12:686–698. https://doi.org/10.1038/nrmicro3326

Burke Watson E, Powell E, Maher NP, Oczkowski AJ, Paudel B, Starke A, Szura K, Wigand C (2018) Indicators of nutrient pollution in Long Island, New York, estuarine environments. Mar Environ Resour 134:109–120. https://doi.org/10.1016/j.marenvres.2018.01.003

Byrd AL, Vlahos P, Whitney MM, Menniti C, Warren JK (2020) Tidally resolved observations of organic carbon exchange through Eastern Long Island Sound. Estuar Coast Shelf Sci 232:1–11. https://doi.org/10.1016/j.ecss.2019.106463

Caffrey JM, Bano N, Kalanetra K, Hollibaugh JT (2007) Ammonia oxidation and ammonia-oxidizing bacteria and archaea from estuaries with differing histories of hypoxia. ISME J 1:660–662. https://doi.org/10.1038/ismej.2007.79

Carstensen J, Anderson JH, Gustafsson BG, Conley DJ (2014) Deoxygenation of the Baltic Sea during the last century. Proc Natl Acad Sci 111(15):5628–5633. https://doi.org/10.1073/pnas.1323156111

Chan F, Barth JA, Kroeker KJ, Lubchenco J, Menge BA (2019) The dynamics and impact of ocean acidification and hypoxia. Oceanography 32(3):62–71

Connecticut Department of Energy and Environmental Protection (CTDEEP), Interstate Environmental Commission, US Environmental Protection Agency (IEC) (2019) 2019 Long Island Sound hypoxia season review. CTDEEP, 1–29. https://portal.ct.gov/-/media/DEEP/water/lis_water_quality/monitoring/2019/FINAL_2019-Combined-Report_april2020.pdf

Connecticut Department of Energy and Environmental Protection (CTDEEP), Interstate Environmental Commission, US Environmental Protection Agency (IEC) (2020) 2020 Long Island Sound hypoxia season review. CTDEEP, 1–50. https://portal.ct.gov/-/media/DEEP/water/lis_water_quality/monitoring/2020/2020-LIS-Combined-Report.pdf

Cuomo C, Valente R, Dogru D (2005) Seasonal variations in sediment and bottom water chemistry of western Long Island Sound: implications for lobster mortality. J Shellfish Res 24(3):805–814. https://doi.org/10.2983/0730-8000(2005)24[805:SVISAB]2.0.CO;2

D'Sa EI, DiMarco SF (2009) Seasonal variability and controls on chromophoric dissolved organic matter in a large river-dominated coastal margin. Limnol Oceanogr 54(6):2233–2242. https://doi.org/10.4319/lo.2009.54.6.2233

Dai M, Guo X, Zhai W, Yan L, Wang B, Wang L, Cai P, Tang T, Cai W (2006) Oxygen depletion in the upper reach of the Pearl River estuary during a winter drought. Mar Chem 102(1–2):159–169. https://doi.org/10.1016/j.marchem.2005.09.020

Daims H, Lücker S, Wagner M (2016) A new perspective on microbes formerly known as nitrite-oxidizing bacteria. Trends Microbiol 24(9):699–712. https://doi.org/10.1016/j.tim.2016.05.004

Diaz RJ, Rosenberg R (2008) Spreading Dead Zones and Consequences for Marine Ecosystems. Sci 321(5891):926–929. https://doi.org/10.1126/science.1156401

Du J, Shen J, Park K, Wang YP, Yu X (2018) Worsened physical condition due to climate change contributes to the increasing hypoxia in Chesapeake Bay. Sci Total Environ 630:707–717. https://doi.org/10.1016/j.scitotenv.2018.02.265

Ducklow HW, Dickson A (1994) Chapter 16: Determination of dissolved organic carbon by a high temperature combustion/direct injection technique. In The Joint Global Ocean Flux study protocols. NOAA. https://www.nodc.noaa.gov/archive/arc0001/9900162/2.2/data/0-data/jgofscd/Files/protocols/chap16.html

Dworkin M, Gutnick D (2012) Sergei Winogradsky: a founder of modern microbiology and the first microbial ecologist. FEMS Microbiol Rev 36(2):264–279. https://doi.org/10.1111/j.1574-6976.2011.00299.x

Dyhrman ST, Ruttenberg KC (2006) Presence and regulation of alkaline phosphatase activity in eukaryotic phytoplankton from the coastal ocean: Implications for dissolved organic phosphorus remineralization. Limnol Oceanogr 51(3):1381–1390. https://doi.org/10.4319/lo.2006.51.3.1381

Egan L, Lachat Applications Group (2007) QuickChem© Method 31-115-01-1-J: Determination of orthophosphate in waters by flow injection analysis colorimetry. Lachat Instruments, 1–32.

Egan L, Lachat Applications Group (2008) QuickChem© Method 31-107-04-1-D: Determination of nitrate and/or nitrite in brackish waters by flow injection analysis. Lachat Instruments, 1–30.

Evans CD, Monteith DT, Cooper DM (2005) Long-term increases in surface water dissolved organic carbon: observations, possible causes and environmental impacts. Environ Pollut 137(1):55–71. https://doi.org/10.1016/j.envpol.2004.12.031

Findlay SEG, Parr TB (2017) Chapter 24: dissolved organic matter. Methods in stream ecology, 3rd edn. Academic Press, pp 21–36

Foster SQ, Fulweiler RW (2019) Estuarine sediments exhibit dynamic and variable biogeochemical responses to hypoxia. J Geophysical Res Biogeosci 124(4):737–758. https://doi.org/10.1029/2018JG004663

Garnier J, Billen G, Cébron A (2007) Modelling nitrogen transformations in the lower Seine River and estuary (France): impact of wastewater release on oxygenation and N_2O emission. Hydrobiologia 588:291–302. https://doi.org/10.1007/s10750-007-0670-1

Gay PS, O'Donnell J, Edwards CA (2004) Exchange between Long Island Sound and adjacent waters. J Geophysical Res Oceans 109(C10):1–15. https://doi.org/10.1029/2004JC002319

Gelesh L, Marshall K, Boicourt W, Lapham L (2016) Methane concentrations increase in bottom waters during summertime anoxia in the highly eutrophic estuary, Chesapeake Bay, USA. Limnol Oceanogr 61(S1):S253–S266. https://doi.org/10.1002/lno.10272

Gieseke A, Prukhold U, Wagner M, Amann R, Schramm A (2001) Community structure and activity dynamics of nitrifying bacteria in a phosphate-removing biofilm. Appl Environ Microbiol 67(3):1351–1362. https://doi.org/10.1128/AEM.67.3.1351-1362.2001

Glibert PM, Al-Azri A, Allen I, Bouwman AF, Beusen AHW, Burford MA, Harrison PJ, Zhou M (2018) Key questions and recent research advances on harmful algal blooms in relation to nutrients and eutrophication. Global ecology and oceanography of harmful algal blooms. Springer, pp 229–259

Gobler CJ, Buck NJ, Sieracki ME, Sañudo-Wilhelmy SA (2006) Nitrogen and silicon limitation of phytoplankton

communities across an urban estuary: the East River-Long Island Sound system. Estuar Coast Shelf Sci 68(1–2):127–138. https://doi.org/10.1016/j.ecss.2006.02.001

Goñi MA, Teixeira MJ, Perkey DW (2003) Sources and distribution of organic matter in a river-dominated estuary (Winyah Bay, SC, USA). Estuar Coast Shelf Sci 57(5–6):1023–1048. https://doi.org/10.1016/S0272-7714(03)00008-8

Grantham BA, Chan F, Nielsen KJ, Fox DS, Barth JA, Huyer A, Lubchenco J, Menge BA (2004) Upwelling-driven nearshore hypoxia signals ecosystem and oceanographic changes in the northeast Pacific. Nat 429:749–754. https://doi.org/10.1038/nature02605

Grasshoff K, Ehrhardt M, Kremling K (1999) Methods of seawater analysis, 3rd edn. Wiley Verlag Chemie GmbH, Weinheim, pp 159–228

Heisler J, Glibert P, Burkholder J, Anderson D, Cochlan W, Dennison W, Dortch Q, Gobler C, Heil C, Humphries E, Lewitus A, Magnien R, Marshall H, Sellner K, Stockwell D, Stoechker D, Suddleson M (2008) Eutrophication and harmful algal blooms: a scientific consensus. Harmful Algae 8(1):3–13. https://doi.org/10.1016/j.hal.2008.08.006

Henriksen K, Kemp WM (1986) Nitrification in estuarine and coastal marine sediments: methods, patterns and regulating factors. In: Blackburn TH, Sørensen J (eds) Nitrogen cycling in coastal marine environments. John Wiley & Sons, New York, pp 207–250

Hollibaugh JT, Gifford SM, Moran M, Ross MJ, Sharma S, Tolar BB (2014) Seasonal variation in the metratranscriptomes of a Thaumarchaeota population from SE USA coastal waters. ISME J 8:685–698. https://doi.org/10.1038/ismej.2013.171

Howarth R, Chan F, Conley DJ, Garnier J, Doney SC, Marino R, Billen G (2011) Coupled biogeochemical cycles: eutrophication and hypoxia in temperate estuaries and coastal marine ecosystems. Frontiers Ecol Environ 9(1):18–26. https://doi.org/10.1890/100008

Intergovernmental Oceanographic Commission (2010) Microscopic and molecular methods for quantitative phytoplankton analysis. In IOC manuals & guides no. 55. UNESCO: Paris, p 110

Iowa State University—Department of Agronomy (2022) IEM computed hourly precipitation totals–NJ. ASOS Network. https://mesonet.agron.iastate.edu/request/asos/hourlyprecip.phtml?network=NJ_ASOS

Jensen LM, Sand-Jensen K, Marcher S, Hansen M (1990) Plankton community respiration along a nutrient gradient in a shallow Danish estuary. Mar Ecol Prog Ser 61:75–85. https://doi.org/10.3354/meps061075

Joint Global Ocean Flux Study (JGOFS) (1996) Chapter 16: Determination of dissolved organic carbon by a high temperature combustion/direct injection technique. In: The Joint Global Ocean Flux study protocols. JGOFS 127–142.

Jun Y, Wenfeng X (2009) Ammonia biofiltration and community analysis of ammonia-oxidizing bacteria in biofilters. Bioresour Technol 100(17):3869–3876. https://doi.org/10.1016/j.biortech.2009.03.021

Kamjunke N, Hertkorn N, Harir M, Schmitt-Kopplin P, Griebler C, Brauns M, Tümpling W, Weitere M, Herzsprung P (2019) Molecular change of dissolved organic matter and patterns of bacterial activity in a stream along a land-use gradient. Water Res 164:114919. https://doi.org/10.1016/j.watres.2019.114919

Könneke M, Bernhard AE, de la Torre JR, Walker CB, Waterbury JB, Stahl DA (2005) Isolation of an autotrophic ammonia-oxidizing marine archaeon. Nat 437:543–546. https://doi.org/10.1038/nature03911

Koppelman LE, Weyl PK, Gross MG, Davies DS (1976) The urban sea: Long Island Sound. Praeger, pp 1–223

Lachat Applications Group (2017) QuickChem© Method 31-107-06-1-B: determination of ammonia in brackish or seawater by flow injection analysis (Rev 2.0). Lachat Instruments, 1–24.

Lapota D, Duckworth D, Word J (2000) Confounding factors in sediment toxicology. Confounding factors in sediment toxicology, 1–19. https://clu-in.org/download/contaminantfocus/sediments/testing-sediments-confound.pdf

Latimer JS, Tedesco MA, Swanson RL, Yarish C, Stacey PE, Garza C (2014) Long Island Sound: prospects for the urban sea. Springer Ser Environ Manage. https://doi.org/10.1007/978-1-4614-6126-5

Lee YJ, Lwiza KMM (2005) Interannual variability of temperature and salinity in shallow water: Long Island Sound. New York J Geophysical Res Oceans 110(C9):1–12. https://doi.org/10.1029/2004JC002507

Lee YJ, Lwiza KMM (2008) Characteristics of bottom dissolved oxygen in Long Island Sound. New York Estuar Coast Shelf Sci 76(2):187–200. https://doi.org/10.1016/j.ecss.2007.07.001

Lehtovirta-Morley LE (2018) Ammonia oxidation: ecology, physiology, biochemistry and why they must all come together. FEMS Microbiol Lett 365(9):1–9. https://doi.org/10.1093/femsle/fny058

Lin S, Wayne Litaker R, Sunda WG (2016) Phosphorus physiology ecology and molecular mechanisms in marine phytoplankton. J Phycology 52(1):10–36. https://doi.org/10.1111/jpy.12365

Liu L, Lwiza KMM, Taylor GT (2015) Importance of the bacterial dynamics in model simulations of seasonal hypoxia. Cont Shelf Res 105:1–17. https://doi.org/10.1016/j.csr.2015.05.008

Logozzo LA, Tzortziou M, Neale P, Clark JB (2021) Photochemical and microbial degradation of chromophoric dissolved organic matter exported from tidal marshes. J Geophysical Res Biogeosci. https://doi.org/10.1029/2020JG005744

Logozzo LA, Martin JW, McArthur J, Raymond PA (2022) Contributions of Fe(III) to UV–Vis absorbance in river water: a case study on the Connecticut River and argument for the systematic tandem measurement of Fe(III) and CDOM. Biogeochemistry 160:17–33. https://doi.org/10.1007/s10533-022-00937-5

Logue JB, Stedmon CA, Kellerman AM, Nielsen NJ, Andersson AF, Laudon H, Lindström ES, Krizberg ES (2016) Experimental insights into the importance of aquatic bacterial community composition to the degradation of dissolved organic matter. ISME J 10:533–545. https://doi.org/10.1038/ismej.2015.131

Lønborg C, Davidson K, Álvarez-Salgado XA, Miller AEJ (2009) Bioavailability and bacterial degradation rates

of dissolved organic matter in a temperate coastal area during an annual cycle. Mar Chem 113(3–4):219–226. https://doi.org/10.1016/j.marchem.2009.02.003

Long Island Sound Study (2015) Long Island Sound Comprehensive Conservation and Management Plan 205—returning the urban sea to abundance. Long Island Sound Study, 1–76. https://longislandsoundstudy.net/wp-content/uploads/2015/09/CCMP_LowRes_Hyperlink_singles.pdf

Long Island Sound Study (2021) Severely hypoxic and anoxic areas. Long Island Sound Study. https://longislandsoundstudy.net/ecosystem-target-indicators/area-of-hypoxia/#:~:text=In%202021a%20severe%20hypoxia%20covered,2021a%20is%2010%20squre%20miles

Lonsdale DJ, Greenfield DI, Hillebrand EM, Nuzzi R, Taylor GT (2006) Contrasting microplanktonic composition and food web structure in two coastal embayments (Long Island, NY, USA). J Plankton Res 28(10):891–905. https://doi.org/10.1093/plankt/fbl027

Mazur CI, Al-Jaj AN, Ray NE, Sanchez-Viruet I, Fulweiler RW (2021) Low denitrification rates and variable benthic nutrient fluxes characterize Long Island Sound sediments. Biogeochemistry 154:37–62. https://doi.org/10.1007/s10533-021-00795-7

Meyer RL, Allen DE, Schmidt S (2008) Nitrification and denitrification as sources of sediment nitrous oxide production: a microsensor approach. Mar Chem 110(1–2):68–76. https://doi.org/10.1016/j.marchem.2008.02.004

Moran MA, Sheldon WM, Sheldon JE (1999) Biodegradation of riverine dissolved organic carbon in five estuaries of the Southeastern United States. Estuaries 22:55–64. https://doi.org/10.2307/1352927

Mosier AC, Francis CA (2010) Denitrifier abundance and activity across the San Francisco Bay estuary. Environ Microbiol 2(5):667–676. https://doi.org/10.1111/j.1758-2229.2010.00156.x

Mullaney JR (2015) Nutrient, organic carbon, and chloride concentrations and loads in selected Long Island Sound tributaries: Four decades of change following the passage of the Federal Clean Water Act: U.S. Geological Survey Scientific Investigations Report 2015–5189, p 47 https://doi.org/10.3133/sir20155189

Naqvi SWA, Bange HW, Farías L, Monteiro PMS, Scranton MI, Zhang J (2010) Marine hypoxia/anoxia as a source of CH_4 and N_2O. Biogeosci 7(7):2159–2190. https://doi.org/10.5194/bg-7-2159-2010

Neubacher EC, Parker RE, Trimmer M (2011) Short-term hypoxia alters the balance of the nitrogen cycle in coastal sediments. Limnol Oceanogr 56(2):651–665. https://doi.org/10.4319/lo.2011.56.2.0651

New York State Department of Environmental Conservation (NYSDEC) (2000) A total maximum daily load analysis to achieve water quality standards for dissolved oxygen in Long Island Sound. NYSDEC—Report, 1–73. https://www.dec.ny.gov/docs/water_pdf/tmdllis.pdf

Ni W, Li M, Ross AC, Najjar RG (2019) Large projected decline in dissolved oxygen in a eutrophic estuary due to climate change. J Geophysical Res Oceans 124(11):8271–8289. https://doi.org/10.1029/2019JC015274

Nicholls JC, Timmer M (2009) Widespread occurrence of the anammox reaction in estuarine sediments. Aquat Microb Ecol 55:105–113. https://doi.org/10.3354/ame01285

Nikon (2015) Nikon NIS-Elements AR (Advanced Research) User's Guide (Ver. 4.50). Laboratory Imaging, spol. s.r.o 1–245. https://www.gvsu.edu/cms4/asset/8FCAC028-902A-3EFC-5137403A360C8843/user_guide_nis-elements_ar.pdf

O'Shea ML, Brosnan TM (2000) Trends in indicators of Eutrophication in Western Long Island Sound and the Hudson-Raritan Estuary. Estuaries 23:877–901. https://doi.org/10.2307/1353004

Parker CA, O'Reilly JE (1991) Oxygen depletion in Long Island Sound: a historical perspective. Estuaries 14:248–264. https://doi.org/10.2307/1351660

Paytan A, McLaughlin K (2007) The oceanic phosphorus cycle. Chem Rev 107(2):563–576. https://doi.org/10.1021/cr0503613

Pearce J, Balcom N (2005) The 1999 Long Island Sound lobster mortality event: findings of the comprehensive research initiative. J Shellfish Res 24(3):691–697. https://doi.org/10.2983/0730-8000(2005)24[691:TLISLM]2.0.CO;2

Porter K, Feig YS (1980) The use of DAPI for identifying and counting aquatic microfloral. Limnol Oceanogr 25(5):943–948. https://doi.org/10.4319/lo.1980.25.5.0943

Rabalais NN, Díaz RJ, Levin LA, Turner RE, Gilbert D, Zhang J (2010) Dynamics and distribution of natural and human-caused hypoxia. Biogeosci 7(2):585–619. https://doi.org/10.5194/bg-7-585-2010

Rabalais NN, Wei-Jun C, Carstensen J, Conley DJ, Fry B, Hu X, Quiñones-Rivera Z, Rosenberg R, Slomp CP, Turner RE, Voss M, Wissel B, Zhang J (2015) Eutrophication-driven deoxygenation in the coastal ocean. Oceanogr 27(1):172–183. https://doi.org/10.5670/oceanog.2014.21

Raymond PA, Bauer JE (2000) Bacterial consumption of DOC during transport through a temperate estuary. Aquat Microb Ecol 22:1–12

Reed ML, DiTullio GR, Kacenas SE, Greenfield DI (2015) Effects of nitrogen and dissolved organic carbon on microplankton abundances in four coastal South Carolina (USA) systems. Aquat Microb Ecol 76:1–14. https://doi.org/10.3354/ame01764

Rich JJ, Dale OR, Song B, Ward BB (2008) Anaerobic ammonium oxidation (anammox) in Chesapeake Bay sediments. Microb Ecol 55:311–320. https://doi.org/10.1007/s00248-007-9277-3

Riverkeeper (2022) East River mid-channel at Roosevelt Island—Entero/Rainfall Table. Riverkeeper. https://www.riverkeeper.org/water-quality/hudson-river/nyc-hudson-bergen/east-river-midchannel-roosevelt/

Sanger DM, Smith EM, Voulgaris G, Koepfler ET, Libes SM, Riekerk GHM, Bergquist DC, Greenfield DI, Wren PA, McCoy CA, Viso RF, Peterson RN, Whitaker JD (2012) Constrained enrichment contributes to hypoxia formation in Long Bay, South Carolina (USA), an open water urbanized coastline. Mar Ecol Prog Ser 461:15–30. https://doi.org/10.3354/meps09796

Santoferrara LF, McManus GB, Greenfield DI, Smith SA (2022) Microbial communities (bacteria, archaea and

eukaryotes) in a temperate estuary during seasonal hypoxia. Aquat Microb Ecol 88:61–79. https://doi.org/10.3354/ame01982

Save the Sound Organization (2022) Long Island Sound Report Card 2022. https://www.savethesound.org/what-we-do/healthy-waters/report-cards-grades/

Schaefer SC, Hollibaugh JT (2017) Temperature decouples ammonium and nitrite oxidation in coastal waters. Environ Sci Technol 51(6):3157–3164. https://doi.org/10.1021/acs.est.6b03483

Schartup AT, Ndu U, Balcom PH, Mason RP, Sunderland EM (2015) Contrasting effects of marine and terrestrially derived dissolved organic matter on mercury speciation and bioavailability in seawater. Environ Sci Technol 49(10):5965–5972. https://doi.org/10.1021/es506274x

Sinha E, Michalak AM, Balaji V (2017) Eutrophication will increase during the 21st century as a result of precipitation changes. Sci 357(6349):405–408. https://doi.org/10.1126/science.aan2409

Sitta KA, Reed M, Mortensen R, Doll C, Callahan T, Greenfield DI (2018) The influences of nitrogen form and zooplankton grazing on phytoplankton assemblages in two coastal southeastern systems. Limnol Oceanogr 64(6):2523–2544. https://doi.org/10.1002/lno.10957

Staniec A, Vlahos P (2017) Timescales for determining temperature and dissolved oxygen trends in the Long Island Sound (LIS) estuary. Cont Shelf Res 151:1–7. https://doi.org/10.1016/j.csr.2017.09.013

Staroscik AM, Smith DC (2004) Seasonal patterns in bacterioplankton abundance and production in Narragansett Bay, Rhode Island, USA. Aquat Microb Ecol 35:275–282. https://doi.org/10.3354/ame035275

Stein LY (2019) Insights into the physiology of ammonia-oxidizing microorganisms. Curr Opin Chem Biol 49:9–15. https://doi.org/10.1016/j.cbpa.2018.09.003

Strickland JDH, Parsons TR (1984) A practical handbook of seawater analysis, 2nd edn. Fisheries Research Board of Canada Bulletin, pp 1–328

Su J, Dai M, He B, Wang L, Gan J, Guo X, Zhao H, Yu F (2017) Tracing the origin of the oxygen-consuming organic matter in the hypoxic zone in a large eutrophic estuary: the lower reach of the Pearl River Estuary, China. Biogeosci 14:4085–4099. https://doi.org/10.5194/bg-14-4085-2017

Su J, Cai W, Brodeur J, Hussain N, Chen B, Testa JM, Scaboo KM, Jaisi DP, Li Q, Dai M, Cornwell J (2020) Source partitioning of oxygen-conusming organic matter in the hypoxic zone of the Chesapeake Bay. Limnol Oceanogr 65(8):1801–1817. https://doi.org/10.1002/lno.11419

Supino JR (2020) Microbial degradability of terrigenous, marsh-exported, and estuarine colored dissolved organic matter in Long Island Sound. Master's Thesis, City College of New York. https://academicworks.cuny.edu/cc_etds_theses/810

Tarayre C, Nguyen H, Brognaux A, Delepierre A, De Clercq L, Charlier R, Michels E, Meers E, Delvigne F (2016) Characterisation of phosphate accumulating organisms and techniques for polyphosphate detection: a review. Sens 16(6):797. https://doi.org/10.3390/s16060797

Taylor GT, Way J, Yu Y, Scranton MI (2003) Ectohydrolase activity in surface waters of the Hudson River and western Long Island Sound estuaries. Mar Ecol Prog Ser 263:1–15. https://doi.org/10.3354/meps263001

Tetra Tech Incorporated (2020) Establishing nitrogen target concentrations for three Long Island Sound watershed groupings: Embayments, large riverian systems, and Western Long Island Sound open water. U.S. Environmental Protection Agency—Region 1 and Long Island Sound Office 1–84. https://longislandsoundstudy.net/wp-content/uploads/2020/10/Subtask-D-Summary-of-Existing-Water-Quality-Data_combined.pdf

Tucker S, Jones D, Lachat Application Group (2008a) © Method 31-107-04-4-B: Determination of total nitrogen in manual persulfate digests for seawater and brackish waters (Low Flow Method). Lachat Instruments, pp 1–36.

Tucker S, Jones D, Lachat Application Group (2008b) © Method 31-115-01-4-B: Determination of total phosphorus in manual persulfate digests for seawater (Low Flow Method). Lachat Instruments, pp 1–36.

Turner Designs (2017) Trilogy laboratory fluorometer user's manual version 1.5, P/N 998–7210. Turner Designs, 1–41.

Tzortziou M, Subramaniam A, Herman JR, Gallegos CL, Neale PJ, Harding LW (2007) Remote sensing reflectance and inherent optical properties in the Mid Chesapeake Bay. Estuar Coast Shelf Sci 7(1–2):16–31. https://doi.org/10.1016/j.ecss.2006.09.018

U.S. Census Bureau (2020) QuickFacts Connecticut and New York. U.S. Census Bureau. https://www.census.gov/quickfacts/CT.

Varekamp J (2010) Environmental change in Long Island Sound in the recent past: Eutrophication and climate change, Long Island Sound report. Grant #CWF 334-R (FRS #525156), pp 1–54. https://people.earth.yale.edu/sites/default/files/files/Thomas/VarekampLobsters2010.pdf

Vaudrey J (2017) New York City's impact on Long Island Sound water quality technical report. University of Connecticut and Save the Sound, pp 1–33

Vaudrey J, Yarish C, Kyun Kim J, Pickerell C, Brousseau L, Eddings J, Sautkulis M (2016) Connecticut Sea Grant Project Report: Comparative analysis and model development for determining the susceptibility to eutrophication of Long Island Sound embayments. Sea Grant, 1–46

Vlahos P, Whitney MM (2017) Organic carbon patterns and budgets in the Long Island Sound estuary. Limnol Oceanogr 62(S1):S46–S57. https://doi.org/10.1002/lno.10638

Vlahos P, Whitney MM, Menniti C, Mullaney JR, Morrison J, Jia Y (2020) Nitrogen budgets of the Long Island Sound estuary. Estuar Coast Shelf Sci 232(106493):1–9. https://doi.org/10.1016/j.ecss.2019.106493

Voss M, Bange HW, Dippner JW, Middelburg JJ, Montoya JP, Ward B (2013) The marine nitrogen cycle: recent discoveries, uncertainties and the potential relevance of climate change. Philos Trans R Soc Lond B 368(1621):1–11. https://doi.org/10.1098/rstb.2013.0121

Walsh J (1995) DOC storage in Arctic seas: the role of continental shelves. In: Smith WO, Grebmeier JM (eds) Arctic oceanography: marginal ice zones and continental

shelves, vol 49. American Geophysical Union, pp 203–230
Weinke AD, Biddanda BA (2018) From bacteria to fish: ecological consequences of seasonal hypoxia in a great lakes estuary. Ecosyst 21:426–442. https://doi.org/10.1007/s10021-017-0160-x
Welsch BL, Eller FC (1991) Mechanisms controlling summertime oxygen depletion in western Long Island Sound. Estuaries 14:265–278. https://doi.org/10.2307/1351661
Welschmeyer N (1994) Fluorometric analysis of chlorophyll a in the presence of chlorophyll b and pheopigments. Limnol Oceanogr 29(8):1985–1992. https://doi.org/10.4319/lo.1994.39.8.1985
Whitney MM, Vlahos P (2021) Reducing hypoxia in an urban estuary despite climate warming. Environ Sci Technol 55(2):941–951. https://doi.org/10.1021/acs.est.0c03964
Wijffels RH, de Gooijer CD, Schepers AW, Tramper J (1996) Immobilized-cell growth: diffusion limitation in expanding micro-colonies. Prog Biotechnol 11:249–256. https://doi.org/10.1016/S0921-0423(96)80034-7
Willey JD, Keiber RJ, Eyman MS, Brooks Avery G (2000) Rainwater dissolved organic carbon: concentrations and global flux. Global Biogeochem Cy 14(1):139–148. https://doi.org/10.1029/1999GB900036
Yang JT, Hsu T, Tan E, Lee K, Krom MD, Kang S, Dai M, Hsiao SS, Yan X, Zou W, Tian L, Kao S (2022) Sedimentary processes dominate nitrous oxide production and emission in the hypoxic zone off the Changjiang River estuary. Sci Total Environ 827(154042):1–12. https://doi.org/10.1016/j.scitotenv.2022.154042
Zhong H, Wang W (2009) Controls of dissolved organic matter and chloride on mercury uptake by a marine diatom. Environ Sci Technol 43(23):8998–9003. https://doi.org/10.1021/es901646k